© 2018. Published by The Company of Biologists Ltd | Development (2018) 145, dev163949. doi:10.1242/dev.163949

RESEARCH ARTICLE

PUF-8 facilitates homologous chromosome pairing by promoting proteasome activity during meiotic entry in *C. elegans*

Ganga Anil Kumar[1,2] and Kuppuswamy Subramaniam[1,*]

ABSTRACT

Pairing of homologous chromosomes is essential for genetic recombination during gametogenesis. In many organisms, chromosome ends are attached to cytoplasmic dynein, and dynein-driven chromosomal movements facilitate the pairing process. Factors that promote or control the cytoskeletal tethering of chromosomes are largely unknown. Here, we show that the conserved RNA-binding protein PUF-8 facilitates the tethering and pairing processes in the *C. elegans* germline by promoting proteasome activity. We have isolated a hypomorphic allele of *pas-1*, which encodes a proteasome core subunit, and find that the homologous chromosomes fail to pair in the *puf-8; pas-1* double mutant due to failure of chromosome tethering. Our results reveal that the *puf-8; pas-1* meiotic defects are caused by the loss of proteasome activity. The axis component HTP-3 accumulates prematurely in the double mutant, and reduction of its activity partially suppresses some of the *puf-8; pas-1* meiotic defects, suggesting that HTP-3 might be an important target of the proteasome in promoting early meiotic events. In summary, our results reveal a role for the proteasome in chromosome tethering and identify PUF-8 as a regulator of proteasome activity during early meiosis.

KEY WORDS: Germ cells, Meiosis, *Caenorhabditis elegans*, *pas-1*, *rpn-1*, *htp-3*

INTRODUCTION

Sexual reproduction depends on the formation of haploid gametes from diploid parent cells. This reduction in ploidy requires accurate segregation of homologous chromosomes (homologs) such that each gamete receives only one set of all chromosomes. Meiosis, a specialized cell division, accomplishes this feat through a series of well-coordinated processes, which include pairing of homologs, assembly of the synaptonemal complex (SC; a complex of proteins that assemble between homologs during meiotic prophase), induction of DNA double-strand breaks (DSBs), crossover formation, resolution of crossovers through homologous recombination, and eventual segregation of paired chromosomes.

A crucial step in the pairing of homologs in many organisms is the cytoplasmic dynein-driven chromosome movements that enable the alignment of homologs. In *C. elegans*, specific repetitive DNA sequences present near one end of each chromosome, known as the pairing centers (PCs), are responsible for attaching chromosome ends to cytoplasmic dynein via the SUN-1/ZYG-12 protein complex that spans the inner and outer nuclear envelopes (NEs) (Penkner et al., 2007; Phillips et al., 2009; Sanford and Perry, 2001; Sato et al., 2009). The pairing event begins when each PC binds to a specific member of a family of zinc-finger proteins comprising ZIM-1, ZIM-2, ZIM-3 and HIM-8 (MacQueen et al., 2005; Phillips and Dernburg, 2006; Phillips et al., 2005). While the PC-binding protein–PC complex binds to SUN-1 at the nuclear periphery, ZYG-12 recruits dynein on the cytoplasmic side (Malone et al., 2003; Penkner et al., 2007; Sato et al., 2009). Upon interaction with the PC complex, the SUN-1/ZYG-12 complex aggregates into foci at specific sites on the NE, which is a hallmark of tethering chromosome ends to cytoskeleton (Sato et al., 2009).

Homolog pairing and synapsis are regulated by two kinases: the checkpoint kinase CHK-2 and the polo-like kinase PLK-2 (Harper et al., 2011; Higashitani et al., 2000; Labella et al., 2011; MacQueen and Villeneuve, 2001). CHK-2 phosphorylates the PC proteins, which then recruit PLK-2 to the PC (Kim et al., 2015). The PC-associated PLK-2, in turn, promotes homolog pairing by an unknown mechanism, and phosphorylates SUN-1, which, although not essential for pairing, is required for continued chromosome movement until pairing and synapsis are complete (Harper et al., 2011; Labella et al., 2011; Woglar et al., 2013). Acting in a feedback fashion, the meiotic chromosome axis components HIM-3 and HTP-1/2 inhibit CHK-2 activity upon proper pairing and synapsis (Kim et al., 2015).

The PUF family RNA-binding proteins are central players in controlling meiotic entry (for a review, see Pushpa et al., 2017). In *C. elegans*, two nearly identical PUF proteins, FBF-1 and FBF-2, promote the proliferative fate by suppressing the expression of both meiotic entry-promoting factors such as *gld-1* and SC components such as HIM-3, HTP-1, HTP-2, SYP-2 and SYP-3 (Crittenden et al., 2002; Merritt and Seydoux, 2010). PUF-8, another *C. elegans* PUF protein, promotes both proliferative and meiotic fates: it prevents premature meiotic entry by facilitating GLP-1/Notch signaling, but also enables germ cells to transition into meiosis by suppressing the RAS/MAPK signaling (Maheshwari et al., 2016; Vaid et al., 2013). PUF proteins control self-renewal/differentiation decisions in other species as well. For example, the *Drosophila* PUF protein Pumilio (Pum) partners with Nanos (Nos) to suppress the expression of differentiation-promoting factors Brain tumor (Brat) and Mei-P26 in germline stem cells (Harris et al., 2011; Joly et al., 2013). In differentiating germ cells known as cystoblasts, in which the Nos level is low and the Brat level is high, Pum partners with Brat and suppresses the translation of Myc, Mad, Medea and Schnurri, which promote the self-renewal fate (Harris et al., 2011; Newton et al., 2015). How the initial meiotic entry decision is coordinated with the execution of early meiotic events – for example, initiation of the pairing process – is not known.

Here, we identify a role for PUF-8 in homolog pairing. We have isolated a hypomorphic allele of *pas-1*, which encodes a core component of the proteasome, and found that the homologous

[1]Department of Biotechnology, Indian Institute of Technology–Madras, Chennai 600036, India. [2]Department of Biological Sciences & Bioengineering, Indian Institute of Technology, Kanpur 208016, India.

*Author for correspondence (subbu@iitm.ac.in)

K.S., 0000-0002-1691-489X

Received 29 January 2018; Accepted 5 March 2018

Development (2018) 145, dev163949. doi:10.1242/dev.163949

chromosomes fail to pair in *puf-8(ok302); pas-1(kp23)* double mutants. Our results revealed that the pairing defect primarily results from the reduction of proteasome activity in the double mutant and that PUF-8 promotes proteasome activity in premeiotic cells. Thus, our results uncover a role for the proteasome in homolog pairing, which is consistent with recent findings (Ahuja et al., 2017; Rao et al., 2017), and identify a molecular link between the meiotic entry decision and the initiation of homolog pairing.

RESULTS

kp23, a mutation that displays a synthetic sterile phenotype with *puf-8*, is a hypomorphic allele of *pas-1*

Even the null alleles of *puf-8*, such as *puf-8(ok302)* and *puf-8(zh17)*, display a temperature-sensitive phenotype: worms homozygous for either of these alleles are sterile at 25°C but fertile at 20°C (Ariz et al., 2009; Subramaniam and Seydoux, 2003). An earlier genetic screen on the *puf-8(zh17)* genetic background identified a number of new mutant alleles that caused sterility even at 20°C when in double-mutant combination with the *puf-8* mutation (Ariz, 2010; Vaid et al., 2013). Here, we describe the characterization of one such mutant allele named *kp23*. Worms homozygous for the *kp23* single mutation did not show any obvious phenotypic defects; they were fertile (*n*=200 worms) with normal brood size and embryonic viability (Fig. S2). Visualization of germline chromatin by DAPI staining revealed that the chromatin morphologies characteristic of germ cells at different developmental stages were also unaffected in *kp23* worms; hermaphrodites produced both sperm and oocytes, and the spermatogenesis in males was unaffected (Fig. 1, Fig. S3). By contrast, *kp23; puf-8* double-mutant hermaphrodites were all sterile (*n*=200 worms); although sperm was present, no oocytes were observed in these worms. Crescent-shaped chromatin morphology, which is characteristic of normal transition zone nuclei, could not be detected in double-mutant germlines. In addition, the chromatin was irregularly distributed and less compact in the pachytene region (Fig. 1). Spermatogenesis in *kp23; puf-8* males was normal, although ∼66% (*n*=346 embryos) of the embryos sired by these males failed to hatch (Fig. S3).

We have mapped *kp23* to the *pas-1* locus using standard two-factor mapping, whole-genome sequencing and RNAi (see the supplementary Materials and Methods for details). *kp23* is a G-to-A missense mutation that substitutes the conserved glycine with glutamic acid at position 20 of the PAS-1 amino acid sequence (Fig. S4). We confirmed the mapping results by generating the same G-to-A mutation in the wild-type strain using the CRISPR/Cas9 genome-editing method; worms homozygous for the resulting allele, *kp72*, did not display any phenotypic defects, and the *puf-8(ok302); pas-1(kp72)* worms shared the same germline defects as *puf-8(ok302); pas-1(kp23)* worms (Fig. S4).

pas-1 encodes the α1 subunit of the 20S proteasome (Davy et al., 2001). Consistent with previous reports (Fernandez et al., 2005; Sonnichsen et al., 2005; Takahashi et al., 2002), depletion of PAS-1 by RNAi resulted in embryonic lethality (data not shown), which prompted us to test whether *kp23* is a hypomorphic allele of *pas-1*. We generated a null allele, *kp73*, by inserting a stop codon followed by an additional frameshift in the first exon of the *pas-1* locus using the CRISPR/Cas9 method. As expected, whereas the worms heterozygous for *kp73* [*pas-1(kp73/+)*] were fertile with normal brood size, the *pas-1(kp73/kp73)* embryos were inviable (Fig. S2).

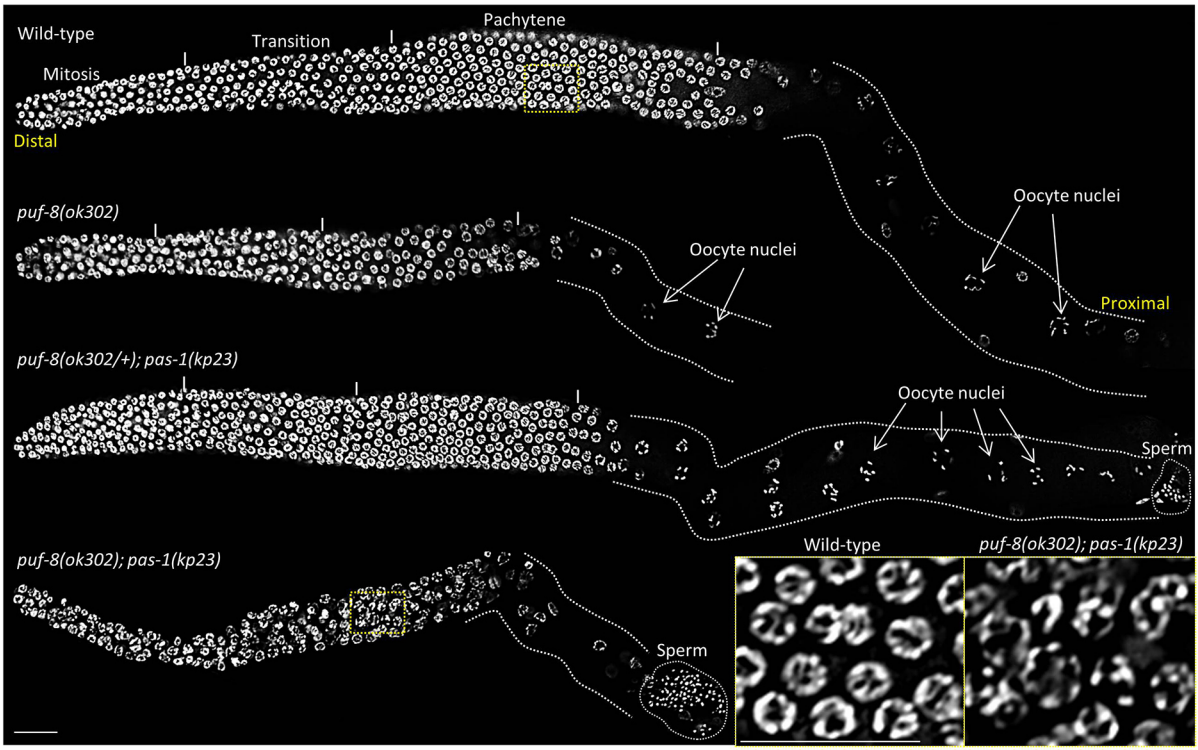

Fig. 1. *puf-8(ok302); pas-1(kp23)* double-mutant gonads lack oocytes. Dissected gonads of the indicated genotypes stained with DAPI. The *C. elegans* gonad is tube shaped and displays a distal (closed end)-proximal polarity with respect to the developmental stages of germ cells. Mitotically cycling germline stem cells and mature gametes are located at the distal and proximal ends, respectively. Approximate boundaries of the mitotic, transition and pachytene regions are indicated (short white lines). Oocytes are absent in the *puf-8(ok302); pas-1(kp23)* double mutant, whereas their nuclei are readily visible in the other three genotypes. Insets show boxed regions (dotted yellow lines) at higher magnification. The double-mutant pachytene chromosomes appear irregularly shaped when compared with the wild type. Scale bars: 20 µm.

Development (2018) 145, dev163949. doi:10.1242/dev.163949

Significantly, *puf-8(ok302/ok302); pas-1(kp73/+)* worms were sterile and produced no oocytes, thus sharing the same phenotypic defects as *puf-8(ok302/ok302); pas-1(kp23/kp23)* (Fig. S5). These results demonstrate that *kp23* is a hypomorphic allele of *pas-1* and that oogenesis in the *puf-8* mutant is sensitive to the reduction of *pas-1* and, by extension, of proteasome activity. Consistent with this notion, depletion of PAS-3, another proteasome component, led to 100% sterility in *puf-8(ok302)* worms (n=200 worms).

We determined the expression pattern of PAS-1 by inserting the coding sequence of GFP in-frame at the C-terminus of PAS-1 at the endogenous *pas-1* locus using CRISPR/Cas9. As shown in Fig. S6A, PAS-1::GFP was present throughout the germline; it was predominantly localized to the nucleus, where it formed alternate bands with the chromatin, as was readily apparent in pachytene nuclei (Fig. S6B).

Homologous chromosomes fail to pair during oogenesis in the *puf-8(ok302); pas-1(kp23)* double mutant

The abnormal meiotic chromatin morphology in *puf-8(ok302); pas-1(kp23)* germlines (Fig. 1) suggested potential meiotic defects, which have been known to trigger apoptosis. Thus, it is possible that the absence of oocytes in *puf-8(ok302); pas-1(kp23)* worms resulted from increased apoptosis. We blocked apoptosis in *puf-8(ok302); pas-1(kp23)* worms by depleting CED-3, a core component of the apoptotic machinery, using RNAi. In wild-type *C. elegans*, oocytes arrest at the diakinetic stage until fertilization. During this stage, the six bivalent chromosomes appear as distinct dots upon staining with DAPI. In the wild type, several immature oocytes, each containing six bivalent chromosomes, accumulated upon CED-3 depletion. Similar observations were made in *puf-8(ok302)* and *pas-1(kp23)* single-mutant germlines as well. Oocytes with seven DAPI dots were occasionally seen in *puf-8(ok302); ced-3(RNAi)* worms, presumably due to the accumulation of defective oocytes that persisted in the absence of apoptosis. In contrast to the *puf-8(ok302); pas-1(kp23)* double mutant, in which oocytes were absent (Fig. 1), several cells resembling diakinetic oocytes were readily observed in *puf-8(ok302); pas-1(kp23); ced-3(RNAi)* germlines; significantly, all these cells contained twelve DAPI dots, suggesting a failure of homolog pairing (Fig. 2). These results indicate that oocytes fail to form in *puf-8(ok302); pas-1(kp23)* worms due to cell death triggered by a potential pairing defect.

As mentioned above, sperm formation was unaffected in *puf-8(ok302); pas-1(kp23)* worms, indicating that meiotic entry was

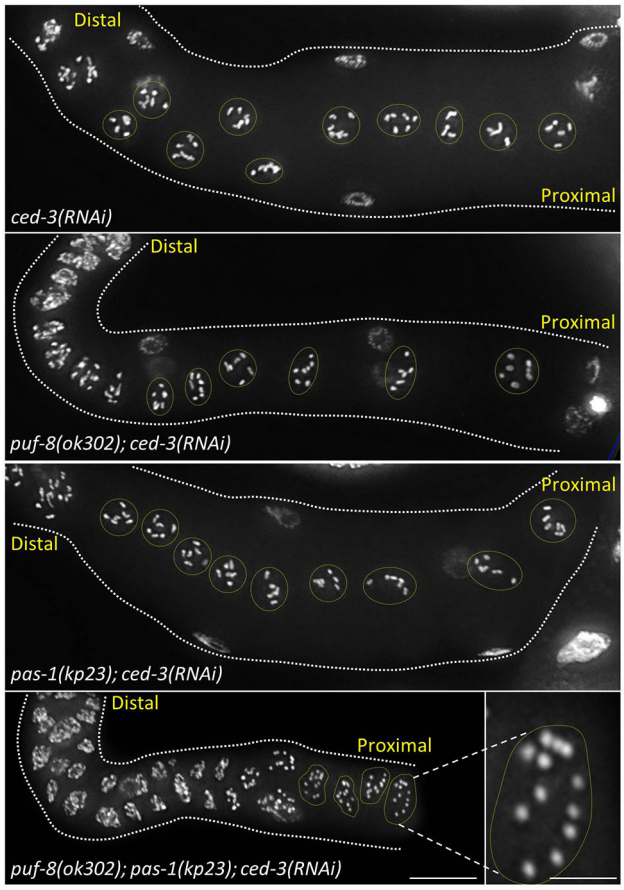

Fig. 2. *puf-8(ok302); pas-1(kp23)* gonads accumulate oocytes with unpaired chromosomes when apoptosis is blocked. Proximal part (diplotene and diakinetic regions) of dissected gonads of the indicated genotypes stained with DAPI. Oocyte nuclei are circled. Most oocyte nuclei in *ced-3(RNAi)*, *puf-8(ok302); ced-3(RNAi)* and *pas-1(kp23); ced-3(RNAi)* possess six DAPI-stained structures representing the six bivalents, whereas 12 such structures are seen in *puf-8(ok302); pas-1(kp23); ced-3(RNAi)* oocytes. Images are maximum intensity projections. Scale bar: 20 µm. Inset shows one oocyte nucleus at higher magnification. Scale bar: 5 µm.

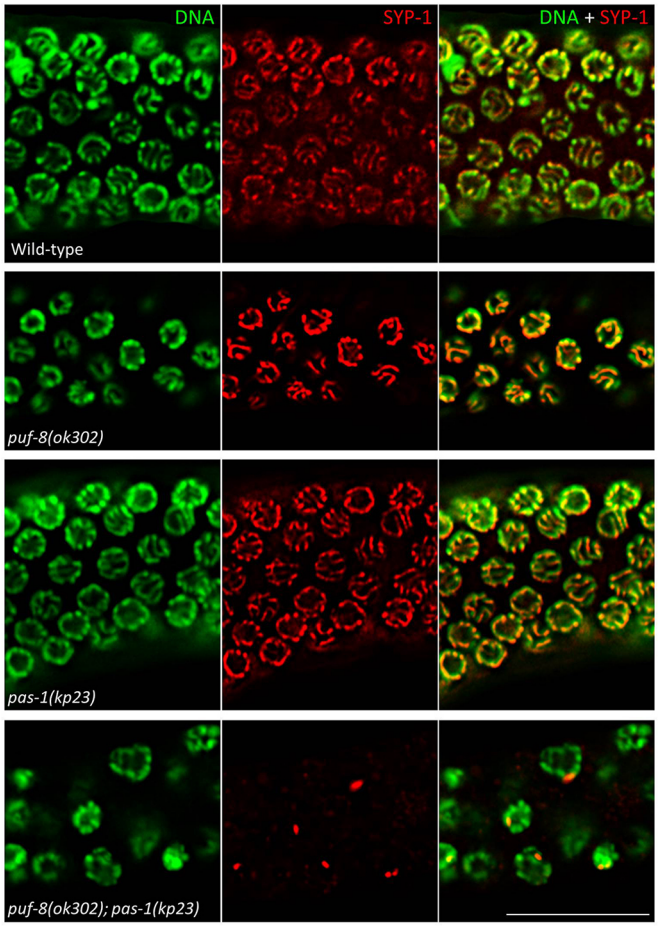

Fig. 3. The synaptonemal complex central element protein SYP-1 fails to spread along chromosomes in *puf-8(ok302); pas-1(kp23)* meiocytes. Sections of pachytene regions of the indicated genotypes stained with DAPI (green) and with anti-SYP-1 antibodies (red). Whereas SYP-1 is seen spread along chromosomes in wild-type, *puf-8(ok302)* and *pas-1(kp23)* nuclei, it aggregates into a single focus in *puf-8(ok302); pas-1(kp23)* nuclei. Scale bar: 20 µm. See Fig. S12 for images of complete gonads.

Development (2018) 145, dev163949. doi:10.1242/dev.163949

unaffected. Nevertheless, we tested by several approaches whether the meiotic entry process was intact in these worms after germ cells switched to the oogenic mode. First, in contrast to the *puf-8(ok302); pas-1(kp23)* double mutant, mutants defective for meiotic entry, such as the *gld-2(q497) gld-1(q485)* and *gap-3(kp1); puf-8(zh17)* double mutants, did not form oocytes upon depletion of CED-3 (Fig. S7) (Kadyk and Kimble, 1998; Vaid et al., 2013). Second, the *puf-8(ok302); pas-1(kp23)* double mutation failed to block tumorigenesis that is dependent on meiotic entry. For example, in the absence of GLD-1 and PUF-8, germ cells in spermatogenic mode dedifferentiate into germ cell tumors only after meiotic entry (Priti and Subramaniam, 2015). The *puf-8(ok302); pas-1(kp23)* worms did form germ cell tumors upon GLD-1 depletion by RNAi (Fig. S8). Oogenic mode germ cells lacking GLD-1 have been shown to dedifferentiate after meiotic entry (Francis et al., 1995). To test the effect of *puf-8(ok302); pas-1(kp23)* on this

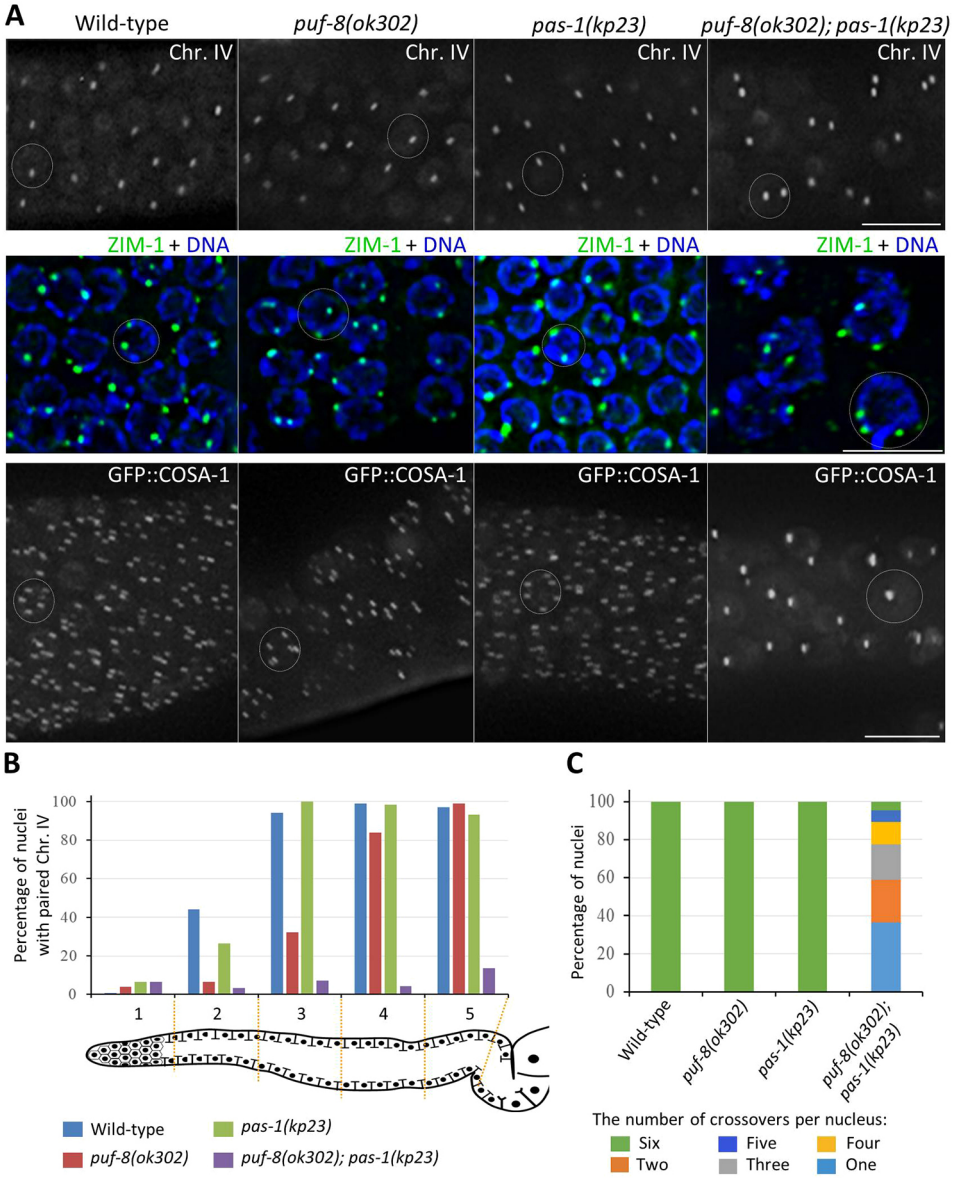

Fig. 4. Homologous chromosomes fail to pair in *puf-8(ok302); pas-1(kp23)* meiocytes. (A) Sections of pachytene regions of the indicated genotypes. (Top) Chromosome IV is visualized using the GFP::LacI fusion protein bound to lacO sequences inserted into chromosome IV. In contrast to the other three genotypes shown, where only one GFP focus representing the paired chromosome IV homologs is seen in each nucleus, two GFP foci are seen in each *puf-8(ok302); pas-1(kp23)* nucleus. (Middle) ZIM-1, which binds to the PCs of chromosomes II and III, is visualized by immunostaining (green); DNA is stained with DAPI (blue). The majority of wild-type, *puf-8(ok302)* and *pas-1(kp23)* germ cells show two ZIM-1 foci per nucleus, which correspond to the bivalents of chromosomes II and III. By contrast, *puf-8(ok302); pas-1(kp23)* nuclei have more than two ZIM-1 foci per nucleus. (Bottom) Crossover sites are visualized using COSA-1::GFP. Six COSA-1::GFP foci per nucleus, corresponding to one crossover per pair of the six homolog pairs, are seen in most wild-type, *puf-8(ok302)* and *pas-1(kp23)* germ cells, whereas only one or two such foci per nucleus, indicating fewer crossovers, are present in *puf-8(ok302); pas-1(kp23)* germ cells. Each oval outlines an individual nucleus. Images in the bottom row are maximum intensity projections. Scale bars: 10 µm. (B) Germlines of the indicated genotypes have been divided into five regions, and the percentage of nuclei in each region with only one GFP::LacI focus (paired chromosome IV) has been plotted. Total nuclei scored for regions 1-5, respectively: 85, 117, 130, 107 and 88 for wild type (four gonads); 49, 78, 87, 95 and 93 for *puf-8(ok302)* (four gonads); 35, 34, 48, 59 and 44 for *pas-1(kp23)* (two gonads); 124, 126, 137, 101 and 55 for *puf-8(ok302); pas-1(kp23)* (six gonads). (C) Numbers of crossovers per nucleus were scored and plotted as percentage of nuclei for the indicated genotypes. Total nuclei scored: 44, 70, 91 and 88 for wild type (three gonads), *puf-8(ok302)* (five gonads), *pas-1(kp23)* (four gonads) and *puf-8(ok302); pas-1(kp23)* (six gonads), respectively.

Development (2018) 145, dev163949. doi:10.1242/dev.163949

gld-1(-)-dependent tumorigenesis, we feminized the hermaphrodite germline by depleting FEM-3, and found that the *gld-1(RNAi); puf-8(ok302); pas-1(kp23) fem-3(RNAi)* animals had well-developed germ cell tumors (Fig. S8). Third, the onset of SUN-1 phosphorylation, which is known to occur upon meiotic entry (Penkner et al., 2009), was unaffected in *puf-8(ok302); pas-1(kp23)* germlines (Fig. S9). Furthermore, chromosomal loading of SC proteins such as HIM-3 and HTP-3 was also intact in the double mutant (see below). These results demonstrate that *puf-8(ok302); pas-1(kp23)* germ cells enter meiosis normally.

To characterize the *puf-8(ok302); pas-1(kp23)* meiotic defects more precisely, we examined the localization patterns of SC proteins and well-known markers of the pairing event. In wild-type meiocytes, the lateral element (axis) components HTP-3 and HIM-3 first appear on the chromatin at the premeiotic stage (Goodyer et al., 2008; Zetka et al., 1999). Although HTP-3 was localized on the chromatin in *puf-8(ok302); pas-1(kp23)* germlines, its localization pattern was more irregular than that seen in the wild type, which is consistent with the abnormal chromatin morphology detected by DAPI staining as described above (Fig. S10). Moreover, unlike the wild type, the double-mutant germlines expressed HTP-3 even in the distalmost germ cells (described in more detail below). The localization pattern of HIM-3 in *puf-8(ok302); pas-1(kp23)* germlines was also suggestive of irregular chromatin morphology. However, the onset of HIM-3 expression, unlike HTP-3, was largely unaffected in these germlines (Fig. S8). The central element protein SYP-1 first appears as foci on a few nuclei just prior to the transition zone and is distributed along the entire length of chromosomes in transition and pachytene zones in the wild type (MacQueen et al., 2002). We obtained similar SYP-1 localization patterns in the *puf-8(ok302)* and *pas-1(kp23)* single-mutant germlines. By contrast, SYP-1 was present only as foci and was never found to form tracks along the chromosomes in *puf-8(ok302); pas-1(kp23)* germlines (Fig. 3, Fig. S12). Similar persistence of SYP-1 foci has been reported in some mutants in which homologous chromosomes fail to pair (Alleva et al., 2017; Bilgir et al., 2013; Brockway et al., 2014; Sato et al., 2009). Thus, consistent with the *ced-3(RNAi)* results described above, the SYP-1 localization defect supports the contention that homolog pairing is defective in *puf-8(ok302); pas-1(kp23)* germlines. We observed a similar localization defect in the case of SYP-2, another central element component (Fig. S13).

Next, we tracked a single chromosome pair (chromosome IV) marked with an integrated bacterial lacO operator sequence using a transgene-expressed GFP::LacI that binds to lacO (Bilgir et al., 2013). As shown in Fig. 4A,B, only one GFP::LacI focus per nucleus, representing paired chromosome IV, was observed in the pachytene zones of wild-type, *puf-8(302)* and *pas-1(kp23)* germlines. By contrast, almost all pachytene nuclei of *puf-8(ok302); pas-1(kp23)* germlines contained two GFP::LacI foci each, which indicates that the homologous chromosomes fail to pair in these germlines. ZIM-1 binds specifically to the PCs on chromosomes II and III. Thus, anti-ZIM-1 antibodies detect two foci, representing the paired chromosomes II and III, in wild-type pachytene nuclei (Phillips and Dernburg, 2006). Whereas we saw only two ZIM-1 foci per nucleus in the pachytene zones of wild-type, *puf-8(ok302)* and *pas-1(kp23)* germlines, there were several nuclei each with three or four ZIM-1 foci in the *puf-8(ok302); pas-1(kp23)* double-mutant pachytene region (Fig. 4A,B).

To confirm the above observations, we detected the crossover sites in all four genotypes using GFP::COSA-1, which binds to the crossover sites (Yokoo et al., 2012). As would be predicted from the single crossover that is known to form per chromosome pair in *C. elegans*, six GFP::COSA-1 foci were present in each late pachytene nucleus in wild-type, *puf-8(ok302)* and *pas-1(kp23)* germlines. By contrast, only one or two GFP::COSA-1 foci were seen in the *puf-8(ok302); pas-1(kp23)* pachytene nuclei (Fig. 4C). These foci appeared larger than those observed in wild type and each single mutant. We conclude that the pairing of homologous chromosomes requires PUF-8 or wild-type PAS-1.

Chromosome ends fail to attach to the cytoskeleton in the *puf-8(ok302); pas-1(kp23)* double mutant

In *C. elegans*, the ends of chromosomes interact with SUN-1 localized on the inner NE, which interacts with ZYG-12 present on the outer NE, which in turn recruits microtubule-associated dynein in the cytoplasm. This chromosomal tethering to the cytoskeleton initiates chromosomal movements that facilitate pairing and synapsis (Penkner et al., 2007; Sato et al., 2009). A hallmark of chromosomal tethering is the formation of ZYG-12 foci on the NE.

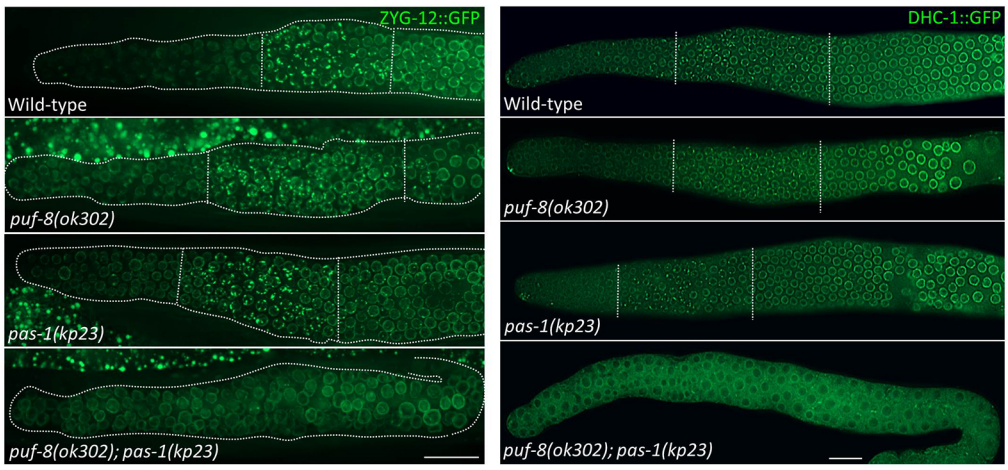

Fig. 5. Chromosome ends fail to attach to the cytoskeleton in *puf-8(ok302); pas-1(kp23)* meiocytes. Aggregation of ZYG-12 and the dynein DHC-1 into distinct foci on the NE indicate successful attachment of homolog pairs to the cytoskeleton. Expression patterns of ZYG-12::GFP (left) and DHC-1::GFP (right) in the germlines of the indicated genotypes are shown. (Left) Maximum intensity projection images of distal arms of gonads (outlined) in intact worms. (Right) Distal arms of dissected gonads. Vertical lines delineate regions of distinct foci visible in wild type, *puf-8(ok302)* and *pas-1(kp23)*; no such distinctions are seen in *puf-8(ok302); pas-1(kp23)* germlines. Scale bars: 20 µm.

Development (2018) 145, dev163949. doi:10.1242/dev.163949

To determine the status of this process in the *puf-8(ok302); pas-1(kp23)* mutant, we examined the localization patterns of ZYG-12 and the dynein heavy chain DHC-1 in live worms using GFP reporter fusions. As expected, both ZYG-12::GFP and DHC-1::GFP formed distinct foci on the NE in transition and early pachytene regions of wild-type, *puf-8(ok302)* and *pas-1(kp23)* germlines (Fig. 5). By contrast, neither of the proteins formed such NE foci in *puf-8(ok302); pas-1(kp23)* germlines, indicating that the chromosome ends fail to attach to the cytoskeleton in these worms.

PUF-8 promotes proteasome activity in the distal germline

Since PAS-1 is a core component of the proteasome and since our genetic analyses (see above) indicate that *pas-1(kp23)* is a reduction-of-function allele, we examined whether proteasome activity is compromised in the *puf-8(ok302); pas-1(kp23)* mutant. We generated a transgenic line that expresses a non-hydrolysable version of ubiquitin fused to a GFP reporter and histone H2B (UbG76V::GFP::H2B) in the germline. Substitution of the C-terminal glycine with valine abrogates hydrolysis of the mutant ubiquitin from substrates conjugated to it, resulting in constitutive targeting of the conjugated substrate for proteasome-mediated degradation (Johnson et al., 1992). The UbG76V mutant form of ubiquitin has previously been shown to be a reliable sensor of proteasome activity in *C. elegans* somatic cells (Hamer et al., 2010). In wild-type germlines, UbG76V::GFP::H2B could not be detected in the mitotic, transition and pachytene zones. Depletion of PAS-1 or PAS-3, another core proteasome component, by RNAi led to the accumulation of UbG76V::GFP::H2B throughout the germline, which demonstrates that the absence of UbG76V::GFP::H2B in the distal germline was indeed due to proteasome-mediated degradation. Presumably due to the absence or low levels of proteasome activity in oocytes, we did detect the presence of UbG76V::GFP::H2B in oocyte nuclei of all genotypes tested. The expression patterns of UbG76V::GFP::H2B in *puf-8(RNAi)* and *pas-1(kp23)* germlines were similar to that of the wild type. By contrast, in *puf-8(RNAi); pas-1(kp23)* germlines, UbG76V::GFP::H2B was readily detectable in the distal germline (Fig. 6). These observations indicate that the *kp23* mutation reduces proteasome activity only partially – the effect was detectable only in the distal part of germlines missing *puf-8* function – and uncover a role for *puf-8* in promoting proteasome activity in the distal germline, where PUF-8 is strongly expressed (Ariz et al., 2009).

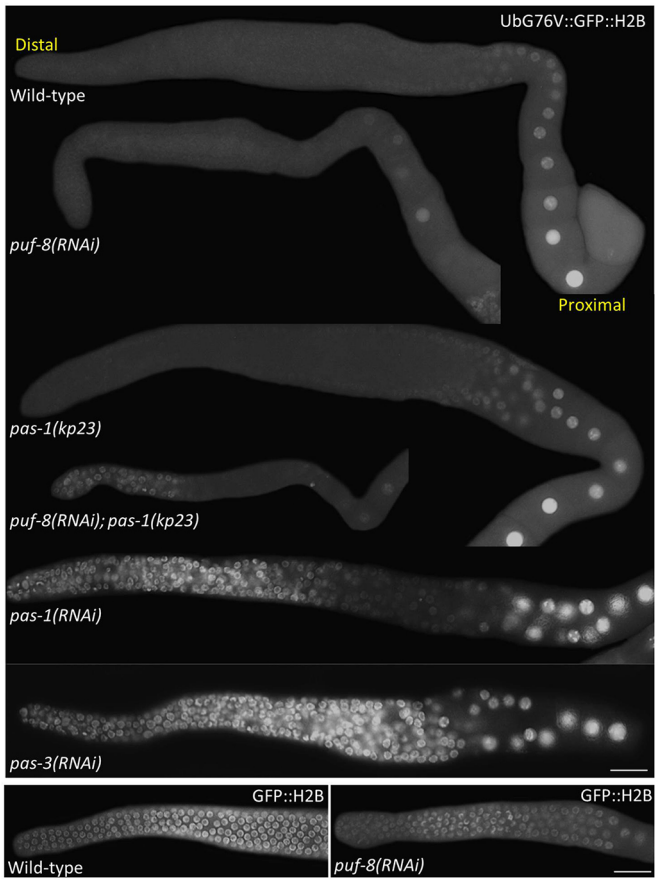

Fig. 6. PUF-8 promotes ubiquitin-mediated protein degradation. Dissected gonads showing the expression patterns of Ub(G76V)::GFP::H2B in germlines of the indicated genotypes. Ub(G76V)::GFP::H2B is expressed in germlines using the *pie-1* promoter and *drp-1* 3′ UTR. Ub(G76V)::GFP::H2B is undetectable from the distal end to the late pachytene region in wild-type, *puf-8(ok302)* and *pas-1(kp23)* germlines. By contrast, Ub(G76V)::GFP::H2B is present in the distal part of *puf-8(ok302); pas-1(kp23)* germlines. Gonads in which the proteasome core components PAS-1 and PAS-3 have been depleted by RNAi are shown as controls for the proteasome-mediated removal of Ub(G76V)::GFP::H2B in the germline. As additional controls, the expression patterns of non-ubiquitylated GFP::H2B, expressed under the same promoter and 3′ UTR, in the wild-type and *puf-8(RNAi)* germlines are shown (bottom). Scale bars: 20 µm.

HTP-3 accumulates precociously in *puf-8(ok302); pas-1(kp23)* germlines

In wild-type germlines, HTP-3 does not accumulate to detectable levels in the mitotic zone. However, when proteasome activity is compromised, the HTP-3 level increases significantly in the mitotic zone, showing that HTP-3 is normally degraded by the proteasome in this zone (Burger et al., 2013). Therefore, if proteasome activity is indeed compromised in the mitotic zone of *puf-8(ok302); pas-1(kp23)* germlines, we would expect HTP-3 to accumulate in this zone. Immunostaining dissected gonads with anti-HTP-3 antibodies revealed that the HTP-3 level in the mitotic zone was substantially higher in the double mutant than in the wild type or the two single mutants (Fig. 7). Thus, these results provide additional evidence that proteasome activity is reduced in the distal part of *puf-8(ok302); pas-1(kp23)* germlines.

Meiotic defects in the *puf-8(ok302); pas-1(kp23)* mutant are due to loss of proteasome activity

Next, we determined whether the *puf-8(ok302); pas-1(kp23)* pairing defect was due to, or independent of, the loss of proteasome activity in the double-mutant germlines. We were able to restore proteasome activity in the double-mutant germline using *kp78*, a mutant allele of *rpn-1*, which encodes a non-ATPase subunit of the proteasome 19S regulatory particle. We isolated *kp78* in a genetic screen for potential suppressors of *puf-8(ok302); pas-1(kp23)* phenotypes (see Materials and Methods and the supplementary Materials and Methods). The *kp78* mutation substitutes a conserved glycine at position 403 to serine and does not cause any obvious phenotypic defects, except a slight reduction in brood size [*rpn-1(kp78)*, 211 progeny/worm, n=5 worms; wild type, 263 progeny/worm, n=6 worms; Fig. S14]. However, *kp78* rescues the sterility phenotype of *puf-8(ok302); pas-1(kp23)* even in the heterozygous condition: all worms of both *puf-8(ok302); rpn-1(kp78/+); pas-1(kp23)* and *puf-8(ok302); rpn-1(kp78/kp78); pas-1(kp23)* genotypes are fertile (n=100 worms; Fig. 8A). In contrast to the *puf-8(ok302); pas-1(kp23)* double mutant, in which UbG76V::GFP::H2B could be readily detected in the first half of the distal germline, it was absent throughout the entire distal part of

Development (2018) 145, dev163949. doi:10.1242/dev.163949

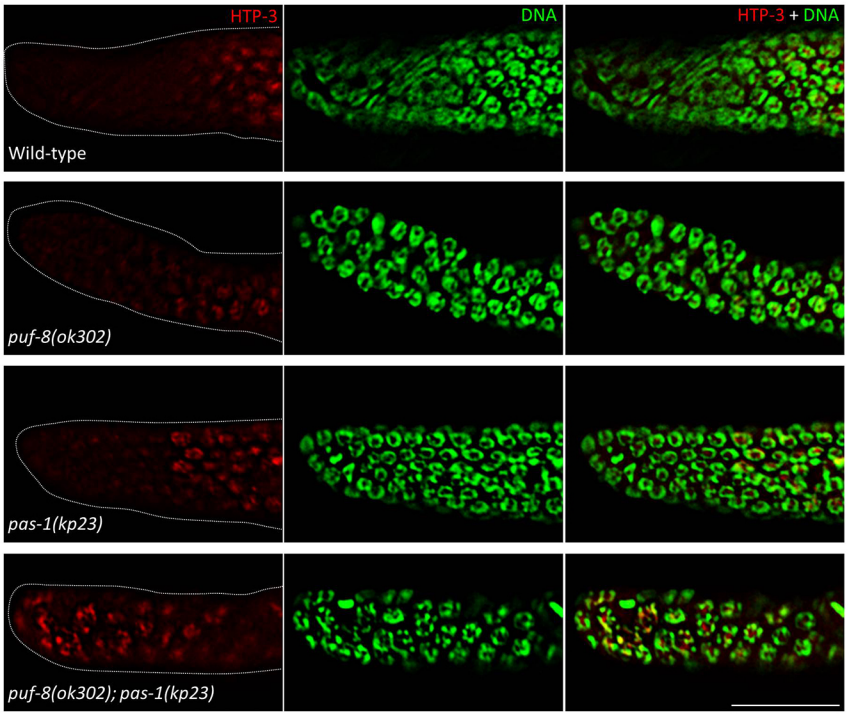

Fig. 7. HTP-3 is expressed precociously in *puf-8(ok302); pas-1(kp23)* germlines. Distal ends of gonads of the indicated genotypes stained with anti-HTP-3 (red) antibodies and DAPI (green). In wild type, *puf-8(ok302)* and *pas-1(kp23)*, HTP-3 expression is weak in the distalmost region of the germline. By contrast, a significant amount of HTP-3 localizes on chromatin in the same region in *puf-8(ok302); pas-1(kp23)* germlines. Scale bar: 20 µm.

triple-mutant germlines (Fig. 8B). Consistently, the HTP-3 expression pattern in the triple mutant was comparable to that of the wild type and unlike that of the *puf-8(ok302); pas-1(kp23)* double mutant (Fig. 8C). These observations strongly support the contention that *rpn-1(kp78)* rescues the proteasome defects caused by the lack of PUF-8 and partial loss of PAS-1 function. Immunostaining revealed normal spreading of SYP-1 along chromosomes in *puf-8(ok302); rpn-1(kp78); pas-1(kp23)* germlines, which is in contrast to the SYP-1 aggregates seen in *puf-8(ok302); pas-1(kp23)* (data not shown). Thus, restoration of proteasome activity abolishes the defective localization patterns of meiotic machinery components such as HTP-3 and SYP-1 and restores fertility in *puf-8(ok302); pas-1(kp23)* worms. The restoration of synapsis in the triple mutant is accompanied by the restoration of chiasmata to homolog pairs, as visualized in the highlighted oocyte nucleus in Fig. 8A. Additionally, depletion of PAS-1 alone by RNAi caused similar SYP-1 aggregation to that observed in *puf-8(ok302); pas-1(kp23)* (Fig. 8D). We conclude that the meiotic defects and sterility observed in these worms are due to the loss or reduction of proteasome activity.

Meiotic defects of the *puf-8(ok302); pas-1(kp23)* mutant are, at least in part, due to increased HTP-3 activity

To investigate how the proteasome contributes to homolog pairing, we first focused on HTP-3 because its expression in the germline, at least its levels in the mitotic zone, is controlled by the proteasome. Moreover, reduction of HTP-3 activity suppresses the sterility phenotype of worms lacking LRR-1, which is the substrate recognition subunit of the E3 ligase $CRL2^{LRR-1}$ that targets HTP-3 for proteasome-mediated degradation (Burger et al., 2013). We tested whether reduction of HTP-3 activity suppressed any of the meiotic defects of *puf-8(ok302); pas-1(kp23)* animals by generating a triple-mutant strain using *vc75*, which is a reduction-of-function allele of *htp-3* (Burger et al., 2013; Couteau and Zetka, 2011). Although the *vc75* mutation did not abolish the misexpression of HTP-3 observed in the *puf-8(ok302); pas-1(kp23)* mitotic zone, the chromatin morphology defects, as revealed by staining with DAPI and anti-HTP-3 antibody, were significantly less severe in *htp-3(vc75); puf-8(ok302); pas-1(kp23)* triple mutants than in *puf-8(ok302); pas-1(kp23)* double mutants (Fig. 9A). This was particularly noticeable in the late pachytene region, where the triple-mutant nuclei exhibited the characteristic wild-type 'bowl of spaghetti' morphology (Fig. 9B). In addition, although the SYP-1 foci persisted longer in the triple mutant than in the wild type, SYP-1 did spread along chromosomes by the time the triple-mutant nuclei progressed to late pachytene stage in 25% of worms (n=133), which is in contrast to *puf-8(ok302); pas-1(kp23)* germlines in which SYP-1 remained as concentrated foci in all worms (n=100) (Fig. 9C). However, the triple mutants did not produce oocytes and were sterile. Thus, the above results suggest that altered HTP-3 expression is at least partly responsible for the meiotic defects of *puf-8(ok302); pas-1(kp23)* mutants.

DISCUSSION

The role of protein degradation during the early events of meiotic prophase I has remained unknown until recently. Earlier this year, Ahuja et al. (2017) showed that the core proteasome is essential in yeast for the homologous coupling of centromeres – a prelude to homolog pairing in yeast – and crossover-dependent repair of the DSB. They also provided evidence that the proteasome is localized on meiotic chromatin and required for SC assembly in both yeast and *C. elegans*. In parallel studies, Rao et al. (2017) showed that SUMO, ubiquitin and the proteasome localize on meiotic chromatin in the mouse, where SUMOylation and ubiquitylation work in tandem to promote DSB repair via crossover formation (Rao et al., 2017). Our current work corroborates these findings and furthermore (1) provides evidence that proteasome activity is essential in *C. elegans* for tethering chromosome ends to the cytoskeleton via SUN-1/ZYG-12, a prerequisite in many organisms for proper homolog pairing, and (2) identifies PUF-8, a conserved translational regulator, as a regulator of proteasome activity in premeiotic cells.

Development (2018) 145, dev163949. doi:10.1242/dev.163949

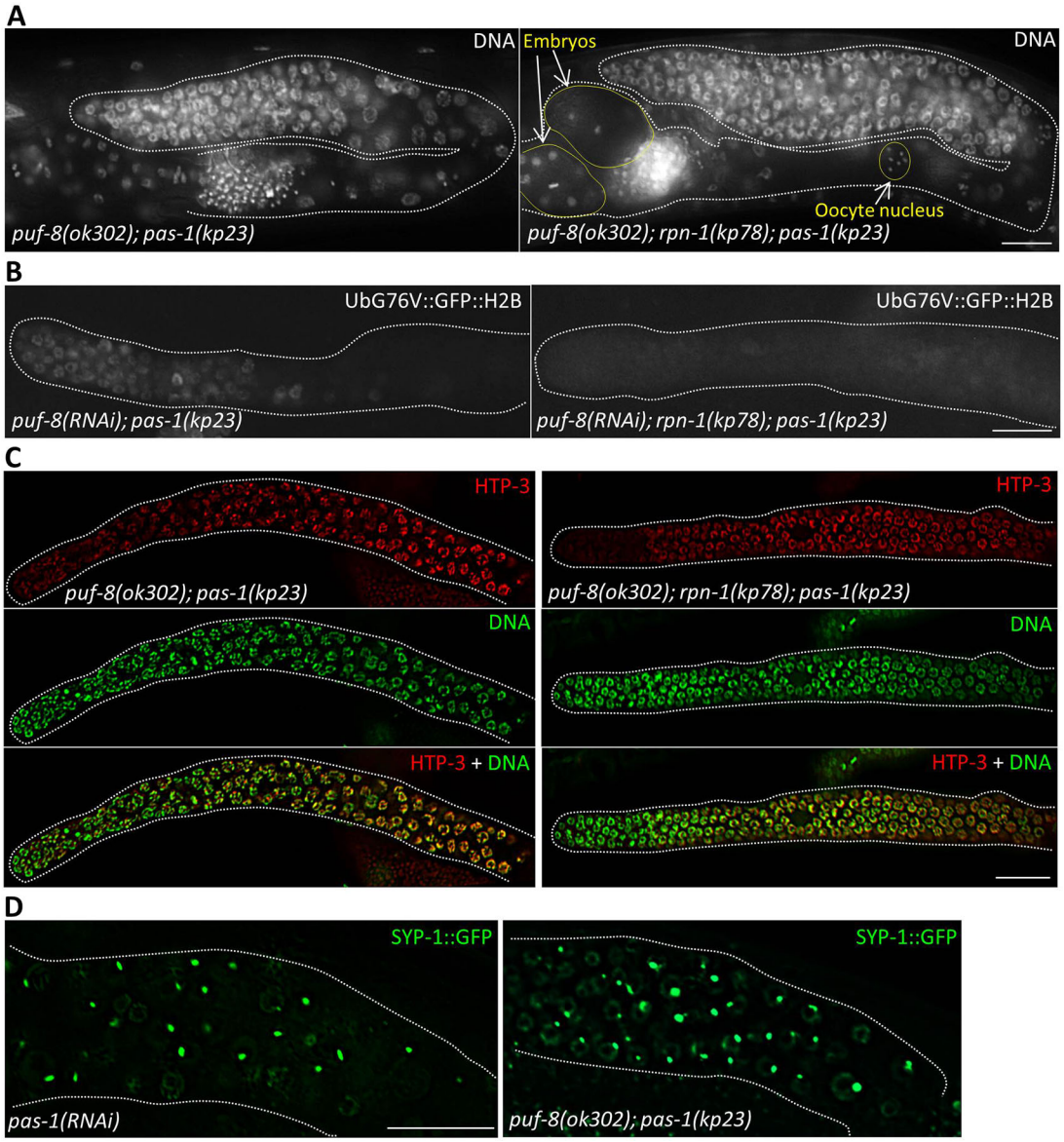

Fig. 8. Meiotic defects of *puf-8(ok302); pas-1(kp23)* are primarily due to loss of proteasome activity. (A) Germlines (white outline) within whole worms of the indicated genotypes, stained with DAPI. Whereas the *puf-8(ok302); pas-1(kp23)* double mutant fails to produce oocytes, the *puf-8(ok302); rpn-1(kp78); pas-1(kp23)* triple mutant produces oocytes and embryos. (B) Expression patterns of Ub(G76V)::GFP::H2B in the distal germline of the indicated genotypes. Proteasome activity, which is significantly reduced in *puf-8(RNAi); pas-1(kp23)* germlines (*n*=80 germlines), is restored by the *kp78* allele of *rpn-1* (*n*=40 germlines). (C) Misexpression of HTP-3 in the mitotic region observed in *puf-8(ok302); pas-1(kp23)* germlines is suppressed by the *kp78* allele. (D) Expression pattern of SYP-1::GFP in the late pachytene region of PAS-1-depleted and *puf-8(ok302); pas-1(kp23)* double-mutant germlines. In both cases, SYP-1::GFP aggregates into foci. Images in D are maximum intensity projections. Scale bars: 20 µm.

Several lines of evidence together demonstrate that the meiotic defects of *puf-8(ok302); pas-1(kp23)* result from loss of proteasome activity in the premeiotic region, rather than being due to a combined effect of reduction of proteasome activity caused by the *kp23* mutation and loss of *puf-8* function that is unrelated to the proteasome. First, depletion of PAS-1 by RNAi causes similar meiotic defects – for example, aggregation of SYP-1 – as seen in *puf-8(ok302); pas-1(kp23)* double mutants. Second, proteasome activity, monitored by detecting the expression of Ub76V::GFP::H2B, is diminished in the *puf-8(ok302); pas-1(kp23)* double-mutant distal germline, but not in either of the single mutants. Third, a potential gain-of-function mutation in *rpn-1*, which encodes a regulatory subunit of the proteasome, restores proteasome activity and suppresses the *puf-8(ok302); pas-1(kp23)* meiotic defects, such that *puf-8(ok302); rpn-1(kp78); pas-1(kp23)* worms are fertile.

In addition to the precocious build-up of a specific proteasome substrate such as HTP-3 in *puf-8(ok302); pas-1(kp23)* germlines, we found that non-hydrolysable ubiquitin fused to a reporter (Ub76V::GFP::H2B) also accumulated in these germlines. These observations indicate that *puf-8* promotes core proteasome activity, rather than promoting the degradation of a specific protein, in the germline. Furthermore, since Ub76V::GFP::H2B accumulated only in the premeiotic region of *puf-8(ok302); pas-1(kp23)* germlines, the positive influence of *puf-8* on the proteasome is spatially restricted to this region, where its expression is strongest (Ariz et al., 2009; Pushpa et al., 2013). Intriguingly, even in this region, the effect of *puf-8* on the proteasome is subtle: neither the HTP-3

Development (2018) 145, dev163949. doi:10.1242/dev.163949

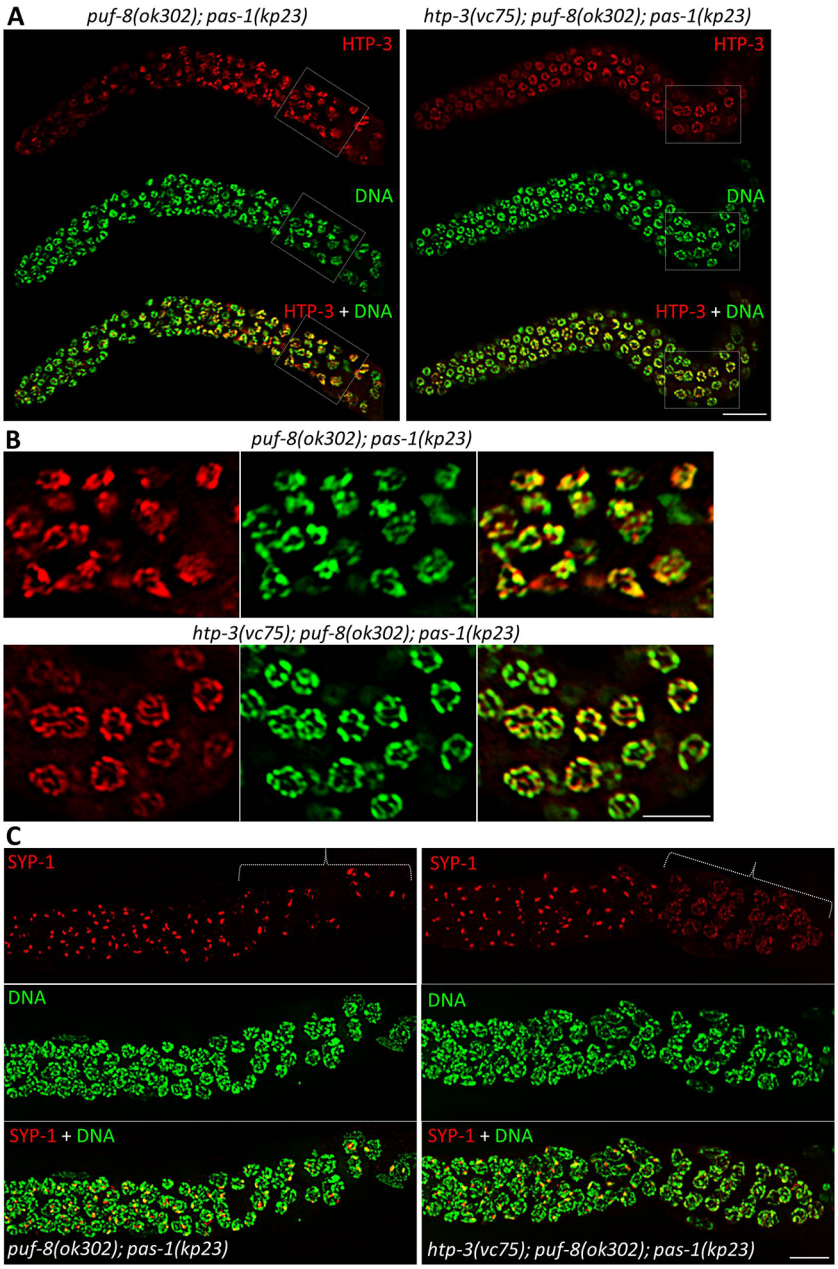

Fig. 9. Reduction of *htp-3* function partly suppresses the morphological defects of *puf-8(ok302); pas-1(kp23)* meiotic chromatin. Dissected gonads of the indicated genotypes stained with DAPI and anti-HTP-3 (A,B) or anti-SYP-1 (C) antibodies. Higher magnifications of the boxed regions in A are shown in B. The chromatin morphology, as revealed by staining with DAPI and anti-HTP-3 antibodies, is more regular – closer to the wild-type 'bowl of spaghetti' morphology (Fig. 3) – in the *htp-3(vc75); puf-8(ok302); pas-1(kp23)* triple mutant than in the *puf-8(ok302); pas-1(kp23)* double mutant. (C) SYP-1 starts to spread along the chromosomes in late pachytene meiocytes of the triple mutant; by contrast, SYP-1 never distributes along chromosomes in the double mutant. The brackets indicate the late pachytene meiocytes. Images in C are maximum intensity projections. Scale bars: 20 µm.

misexpression nor the accumulation of Ub76V::GFP::H2B was observed in *puf-8* single mutants, although meiotic defects were observed in these worms (Subramaniam and Seydoux, 2003). We have previously reported a similar subtle, but negative, influence of *puf-8* on RAS/MAPK signaling in promoting mitotic exit (Vaid et al., 2013). Thus, these observations support the conclusion that PUF-8 primarily functions as a regulator, rather as an absolute on/off switch, in facilitating the mitosis-meiosis transition. Such a role is likely to be crucial to control the number of germ cells that enter meiosis at any given time, which, in turn, is potentially crucial for maintaining the size of the self-renewing population.

How does *puf-8* regulate core proteasome activity? Since PUF-8 regulates the translation of specific mRNAs (Maheshwari et al., 2016; Mainpal et al., 2011; Vaid et al., 2013), an obvious possibility is that it regulates the translation of one or more of the core components of the proteasome. Alternatively, expression of factor(s) that regulate proteasome activity, such as RPN-1, might be subject to translational control by PUF-8. A third possibility is that PUF-8 controls the stability of one or more mRNAs connected to proteasome activity or regulation (Pushpa et al., 2013). The transgenic line expressing Ub76V::GFP::H2B in the germline, generated in the current work, will be a valuable resource in screening for the relevant mRNA(s).

Multiple observations reported here – unpaired chromosome IV, presence of more than two ZIM-1 foci, severe reduction in the number of COSA-1 foci that mark the crossovers, and SYP-1 aggregation – provide evidence that homologous chromosomes fail to pair in *puf-8(ok302); pas-1(kp23)* animals. An early event during homolog pairing is the binding of PC proteins such as ZIM-1 to PCs, which was not affected in these animals. Thus, proteasome activity might not be essential for the PC-binding protein–PC interaction. A crucial subsequent event is the initiation of pairing, upon which the PC proteins bound to a given homolog pair appear as a single focus. The paired PCs are tethered to the cytoplasmic

Development (2018) 145, dev163949. doi:10.1242/dev.163949

microtubule-associated dynein via the SUN-1/ZYG-12 proteins, which leads to aggregation of ZYG-12 and the dynein DHC-1 to form specific foci on the NE (Penkner et al., 2007; Sato et al., 2009). In the *puf-8(ok302); pas-1(kp23)* mutant, the PCs do not pair and neither ZYG-12 nor DHC-1 forms specific foci, which suggests that an intact proteasome is essential for initiating the pairing process. Although the proteasome substrate(s) most relevant to the pairing process are currently unknown, our observations that the axis protein HTP-3 prematurely accumulates in *puf-8(ok302); pas-1(kp23)* germlines and that the reduction of HTP-3 activity partially rescues chromatin morphology and promotes SYP-1 spreading along chromosomes, suggest that the proteasome contributes to homolog pairing and synapsis, at least in part, by preventing the premature accumulation of HTP-3 in mitotic/premeiotic germ cells.

MATERIALS AND METHODS

C. elegans strains

All strains were maintained at 20°C as described (Brenner, 1974). We used the Bristol (N2) strain as the wild type. Strains used are listed in Table S1. Genetic mapping of *kp23* and *kp78* mutations and the generation of various transgenic lines and genetic mutant combinations used in this study are described in the supplementary Materials and Methods, Figs S1 and S11.

Fluorescence microscopy

Whole worms and dissected gonads were stained with DAPI to visualize DNA as described previously (Francis et al., 1995). For immunostaining, gonads were dissected, permeabilized by freeze-crack, fixed and incubated with antibodies as described (Ariz et al., 2009). Fixation conditions were as described by MacQueen et al. (2005). The following antibodies were used: anti-pSUN-1 (Penkner et al., 2009), anti-SYP-1 (MacQueen et al., 2002), anti-ZIM-1 (Phillips and Dernburg, 2006) and anti-HTP-3 (Goodyer et al., 2008) at 1:1000, 1:1000, 1:500 and 1:250, respectively. Secondary antibodies were from Jackson ImmunoResearch Laboratories and used at 1:50. Immunostained gonads were mounted in Vectashield (Vector Laboratories) anti-fading agent before microscopy. Fluorescence signals of immunostained gonads and those expressing GFP were observed using a Zeiss Axio Imager M2 fluorescence microscope. Images were captured using a CCD camera (Zeiss Axiocam 506 Mono) and deconvolved using the Deconvolution module of Axiovision software (Zeiss).

Mutagenesis

To identify mutations that suppress the *puf-8(ok302); pas-1(kp23)* phenotype, the IT1028 [*puf-8(ok302) unc-4(e120)/mnC1 II; pas-1(kp23) V*] strain was treated with the chemical mutagen ethyl methanesulfonate (EMS) as described (Brenner, 1974). Briefly, L4 larvae were incubated in M9 buffer (22 mM KH_2PO_4, 42 mM Na_2HPO_4, 85 mM NaCl, 1 mM $MgSO_4$, pH 7.0) containing 50 mM EMS for 6 h, washed and allowed to recover on lawns of *E. coli* strain OP50. After 12 h, embryos were collected from gravid hermaphrodites. Larvae hatching out of these F1 embryos were cloned and their progeny examined. F1 clones producing fertile *puf-8(ok302) unc-4(e120); pas-1(kp23)* progeny, which were identified based on the uncoordinated phenotype, were selected as carrying potential suppressor mutations.

RNA interference

For RNAi, 500-700 bp coding sequences were PCR amplified from cDNA synthesized from total RNA isolated from wild-type worms and were cloned into the pSV2 vector (Mainpal et al., 2011). PCR primers used for *pas-1*, *pas-3*, *uig-1* and *coh-3* RNAi clones are listed in Table S2; the *puf-8* RNAi clone was already available (Mainpal et al., 2011). For RNAi treatment, worms were grown on lawns of *E. coli* strain HT115 carrying the desired pSV2 construct as described (Mainpal et al., 2011). Since loss of PAS-1 or PAS-3 causes embryonic lethality, L2 stage larvae were transferred to RNAi lawns and the phenotypes were scored at the adult stage of the same worms. For *uig-1* and *coh-3*, L4 larvae were transferred to RNAi lawns and their progeny examined for the RNAi phenotype.

Generation of point mutations and reporter insertions

Various point mutations and reporter insertions were introduced by the CRISPR/Cas9 genome-editing method using protocols described by Arribere et al. (2014). To drive sgRNA expression in *C. elegans*, we constructed a new plasmid vector, pAP20, which does not have the concatamerization problem observed with pRB1017 as described by Arribere et al. (2014). We removed the internal *Bsa*I site in pSV2 by digestion with *Bsa*I and *Bgl*II and religation, and inserted the sgRNA expression cassette containing a U6 promoter, two *Bsa*I sites and the sequence for coding tracrRNA at the *Eco*RV site to yield pAP20. The sgRNA cassette was PCR amplified using primers KS4973 and KS4974 from pRB1017 (Arribere et al., 2014). Annealed oligonucleotides coding for sgRNAs were ligated to *Bsa*I-digested pAP20. The pAP20 vector was used to express sgRNAs for all edits except for generating the *pas-1(kp72)* mutation for which the pDD162 vector was used (Dickinson et al., 2013). We used pJA58 as the sgRNA template targeting the *dpy-10* locus as the co-injection marker (Arribere et al., 2014).

We used single-stranded oligodeoxynucleotides (ssODNs) as repair templates (Paix et al., 2014) for introducing point mutations and the long homology-dependent repair method (Dickinson et al., 2015) for GFP insertion. We PCR amplified the GFP coding sequences from pKS114 (Mainpal et al., 2011) using primers KS4194 and KS5423 and inserted at the *Xma*I site of pBluescript KS(+) (Stratagene) to generate pAK96. About 600 bp sequences immediately upstream [5′ homology arm (HA)] and downstream (3′ HA) of the PAS-1 stop codon were PCR amplified from genomic DNA obtained from wild-type worms using the primer pairs KS5576+KS5577 and KS5578+KS5579, respectively. The PCR products were cloned at *Bam*HI and *Hin*dIII sites of pAK96, respectively, to generate the repair template pAK115 for inserting GFP downstream of the *pas-1* coding sequence. For generating the IT1187 strain, which expresses Ub(G76V)::GFP::H2B, the coding sequence of Ub(G76V) was PCR amplified from the AGD1033 strain (Vilchez et al., 2012) using primers KS5432 and KS5433 and the PCR product was used as the repair template. Ub(G76V) coding sequences were introduced upstream of the GFP coding sequences in the IT828 strain, which carries an integrated transgene that expresses GFP::H2B under the control of the *pie-1* promoter and *drp-1* 3′ UTR (A. Chaturbedi and K.S., unpublished). All oligonucleotides mentioned above are listed in Table S2.

Acknowledgements

We thank Abby Dernburg for anti-SYP-1, anti-ZIM-1 and anti-HTP-3 antibodies; Verena Jantsch for pSUN-1 antibodies; Monique Zetka for the *htp-3(vc75)* strain; Joshua Arribere and Andrew Fire for the pRB1017 plasmid; Dominique Rasoloson and Geraldine Seydoux for pDD162 and pJA58 plasmids; and Lionel Pintard for information on the *vc75* allele. Some of the *C. elegans* strains used in this study were provided by the *Caenorhabditis* Genetics Center, which is funded by National Institutes of Health Office of Research Infrastructure Programs (P40 OD010440).

Competing interests

The authors declare no competing or financial interests.

Author contributions

Conceptualization: G.A.K., K.S.; Methodology: G.A.K., K.S.; Validation: G.A.K., K.S.; Formal analysis: G.A.K., K.S.; Investigation: G.A.K., K.S.; Resources: K.S.; Writing - original draft: G.A.K., K.S.; Writing - review & editing: K.S.; Supervision: K.S.; Project administration: K.S.; Funding acquisition: K.S.

Funding

Research in the K.S. laboratory is supported by grants from the Department of Biotechnology, Ministry of Science and Technology (BT/PR11893/BRB/10/1322/2014) and the Department of Science and Technology, Ministry of Science and Technology (SB/SO/BB-0087/2013), Government of India.

Supplementary information

Supplementary information available online at
http://dev.biologists.org/lookup/doi/10.1242/dev.163949.supplemental

References

Ahuja, J. S., Sandhu, R., Mainpal, R., Lawson, C., Henley, H., Hunt, P. A., Yanowitz, J. L. and Börner, G. V. (2017). Control of meiotic pairing and recombination by chromosomally tethered 26S proteasome. *Science* **355**, 408-411.

Alleva, B., Balukoff, N., Peiper, A. and Smolikove, S. (2017). Regulating chromosomal movement by the cochaperone FKB-6 ensures timely pairing and synapsis. *J. Cell Biol.* **216**, 393-408.

Ariz, M. (2010). Identifying partners of PUF-8, a C. elegans member of the PUF family of RNA-binding proteins. *PhD thesis*, Indian Institute of Technology, Kanpur, India.
Ariz, M., Mainpal, R. and Subramaniam, K. (2009). C. elegans RNA-binding proteins PUF-8 and MEX-3 function redundantly to promote germline stem cell mitosis. *Dev. Biol.* **326**, 295-304.
Arribere, J. A., Bell, R. T., Fu, B. X. H., Artiles, K. L., Hartman, P. S. and Fire, A. Z. (2014). Efficient marker-free recovery of custom genetic modifications with CRISPR/Cas9 in Caenorhabditis elegans. *Genetics* **198**, 837-846.
Bilgir, C., Dombecki, C. R., Chen, P. F., Villeneuve, A. M. and Nabeshima, K. (2013). Assembly of the synaptonemal complex is a highly temperature-sensitive process that is supported by PGL-1 during Caenorhabditis elegans meiosis. *G3 (Bethesda)* **3**, 585-595.
Brenner, S. (1974). The genetics of Caenorhabditis elegans. *Genetics* **77**, 71-94.
Brockway, H., Balukoff, N., Dean, M., Alleva, B. and Smolikove, S. (2014). The CSN/COP9 signalosome regulates synaptonemal complex assembly during meiotic prophase I of Caenorhabditis elegans. *PLoS Genet.* **10**, e1004757.
Burger, J., Merlet, J., Tavernier, N., Richaudeau, B., Arnold, A., Ciosk, R., Bowerman, B. and Pintard, L. (2013). CRL2(LRR-1) E3-ligase regulates proliferation and progression through meiosis in the Caenorhabditis elegans germline. *PLoS Genet.* **9**, e1003375.
Couteau, F. and Zetka, M. (2011). DNA damage during meiosis induces chromatin remodeling and synaptonemal complex disassembly. *Dev. Cell* **20**, 353-363.
Crittenden, S. L., Bernstein, D. S., Bachorik, J. L., Thompson, B. E., Gallegos, M., Petcherski, A. G., Moulder, G., Barstead, R., Wickens, M. and Kimble, J. (2002). A conserved RNA-binding protein controls germline stem cells in Caenorhabditis elegans. *Nature* **417**, 660-663.
Davy, A., Bello, P., Thierry-Mieg, N., Vaglio, P., Hitti, J., Doucette-Stamm, L., Thierry-Mieg, D., Reboul, J., Boulton, S., Walhout, A. J. M. et al. (2001). A protein-protein interaction map of the Caenorhabditis elegans 26S proteasome. *EMBO Rep.* **2**, 821-828.
Dickinson, D. J., Ward, J. D., Reiner, D. J. and Goldstein, B. (2013). Engineering the Caenorhabditis elegans genome using Cas9-triggered homologous recombination. *Nat. Methods* **10**, 1028-1034.
Dickinson, D. J., Pani, A. M., Heppert, J. K., Higgins, C. D. and Goldstein, B. (2015). Streamlined genome engineering with a self-excising drug selection cassette. *Genetics* **200**, 1035-1049.
Fernandez, A. G., Gunsalus, K. C., Huang, J., Chuang, L. S., Ying, N., Liang, H. L., Tang, C., Schetter, A. J., Zegar, C., Rual, J. F. et al. (2005). New genes with roles in the C. elegans embryo revealed using RNAi of ovary-enriched ORFeome clones. *Genome Res.* **15**, 250-259.
Francis, R., Barton, M. K., Kimble, J. and Schedl, T. (1995). gld-1, a tumor suppressor gene required for oocyte development in Caenorhabditis elegans. *Genetics* **139**, 579-606.
Goodyer, W., Kaitna, S., Couteau, F., Ward, J. D., Boulton, S. J. and Zetka, M. (2008). HTP-3 links DSB formation with homolog pairing and crossing over during C. elegans meiosis. *Dev. Cell* **14**, 263-274.
Hamer, G., Matilainen, O. and Holmberg, C. I. (2010). A photoconvertible reporter of the ubiquitin-proteasome system in vivo. *Nat. Methods* **7**, 473-478.
Harper, N. C., Rillo, R., Jover-Gil, S., Assaf, Z. J., Bhalla, N. and Dernburg, A. F. (2011). Pairing centers recruit a Polo-like kinase to orchestrate meiotic chromosome dynamics in C. elegans. *Dev. Cell* **21**, 934-947.
Harris, R. E., Pargett, M., Sutcliffe, C., Umulis, D. and Ashe, H. L. (2011). Brat promotes stem cell differentiation via control of a bistable switch that restricts BMP signaling. *Dev. Cell* **20**, 72-83.
Higashitani, A., Aoki, H., Mori, A., Sasagawa, Y., Takanami, T. and Takahashi, H. (2000). Caenorhabditis elegans Chk2-like gene is essential for meiosis but dispensable for DNA repair. *FEBS Lett.* **485**, 35-39.
Johnson, E. S., Bartel, B., Seufert, W. and Varshavsky, A. (1992). Ubiquitin as a degradation signal. *EMBO J.* **11**, 497-505.
Joly, W., Chartier, A., Rojas-Rios, P., Busseau, I. and Simonelig, M. (2013). The CCR4 deadenylase acts with Nanos and Pumilio in the fine-tuning of Mei-P26 expression to promote germline stem cell self-renewal. *Stem Cell Reports* **1**, 411-424.
Kadyk, L. C. and Kimble, J. (1998). Genetic regulation of entry into meiosis in Caenorhabditis elegans. *Development* **125**, 1803-1813.
Kim, Y., Kostow, N. and Dernburg, A. F. (2015). The chromosome axis mediates feedback control of CHK-2 to ensure crossover formation in C. elegans. *Dev. Cell* **35**, 247-261.
Labella, S., Woglar, A., Jantsch, V. and Zetka, M. (2011). Polo kinases establish links between meiotic chromosomes and cytoskeletal forces essential for homolog pairing. *Dev. Cell* **21**, 948-958.
MacQueen, A. J. and Villeneuve, A. M. (2001). Nuclear reorganization and homologous chromosome pairing during meiotic prophase require C. elegans chk-2. *Genes Dev.* **15**, 1674-1687.
MacQueen, A. J., Colaiacovo, M. P., McDonald, K. and Villeneuve, A. M. (2002). Synapsis-dependent and -independent mechanisms stabilize homolog pairing during meiotic prophase in C. elegans. *Genes Dev.* **16**, 2428-2442.
MacQueen, A. J., Phillips, C. M., Bhalla, N., Weiser, P., Villeneuve, A. M. and Dernburg, A. F. (2005). Chromosome sites play dual roles to establish homologous synapsis during meiosis in C. elegans. *Cell* **123**, 1037-1050.
Maheshwari, R., Pushpa, K. and Subramaniam, K. (2016). A role for post-transcriptional control of endoplasmic reticulum dynamics and function in C. elegans germline stem cell maintenance. *Development* **143**, 3097-3108.
Mainpal, R., Priti, A. and Subramaniam, K. (2011). PUF-8 suppresses the somatic transcription factor PAL-1 expression in C. elegans germline stem cells. *Dev. Biol.* **360**, 195-207.
Malone, C. J., Misner, L., Le Bot, N., Tsai, M. C., Campbell, J. M., Ahringer, J. and White, J. G. (2003). The C. elegans hook protein, ZYG-12, mediates the essential attachment between the centrosome and nucleus. *Cell* **115**, 825-836.
Merritt, C. and Seydoux, G. (2010). The Puf RNA-binding proteins FBF-1 and FBF-2 inhibit the expression of synaptonemal complex proteins in germline stem cells. *Development* **137**, 1787-1798.
Newton, F. G., Harris, R. E., Sutcliffe, C. and Ashe, H. L. (2015). Coordinate post-transcriptional repression of Dpp-dependent transcription factors attenuates signal range during development. *Development* **142**, 3362-3373.
Paix, A., Wang, Y., Smith, H. E., Lee, C.-Y. S., Calidas, D., Lu, T., Smith, J., Schmidt, H., Krause, M. W. and Seydoux, G. (2014). Scalable and versatile genome editing using linear DNAs with microhomology to Cas9 Sites in Caenorhabditis elegans. *Genetics* **198**, 1347-1356.
Penkner, A., Tang, L., Novatchkova, M., Ladurner, M., Fridkin, A., Gruenbaum, Y., Schweizer, D., Loidl, J. and Jantsch, V. (2007). The nuclear envelope protein Matefin/SUN-1 is required for homologous pairing in C. elegans meiosis. *Dev. Cell* **12**, 873-885.
Penkner, A. M., Fridkin, A., Gloggnitzer, J., Baudrimont, A., Machacek, T., Woglar, A., Csaszar, E., Pasierbek, P., Ammerer, G., Gruenbaum, Y. et al. (2009). Meiotic chromosome homology search involves modifications of the nuclear envelope protein Matefin/SUN-1. *Cell* **139**, 920-933.
Phillips, C. M. and Dernburg, A. F. (2006). A family of zinc-finger proteins is required for chromosome-specific pairing and synapsis during meiosis in C. elegans. *Dev. Cell* **11**, 817-829.
Phillips, C. M., Wong, C., Bhalla, N., Carlton, P. M., Weiser, P., Meneely, P. M. and Dernburg, A. F. (2005). HIM-8 binds to the X chromosome pairing center and mediates chromosome-specific meiotic synapsis. *Cell* **123**, 1051-1063.
Phillips, C. M., Meng, X., Zhang, L., Chretien, J. H., Urnov, F. D. and Dernburg, A. F. (2009). Identification of chromosome sequence motifs that mediate meiotic pairing and synapsis in C. elegans. *Nat. Cell Biol.* **11**, 934-942.
Priti, A. and Subramaniam, K. (2015). PUF-8 functions redundantly with GLD-1 to promote the meiotic progression of spermatocytes in caenorhabditis elegans. *G3 (Bethesda)* **5**, 1675-1684.
Pushpa, K., Kumar, G. A. and Subramaniam, K. (2013). PUF-8 and TCER-1 are essential for normal levels of multiple mRNAs in the C. elegans germline. *Development* **140**, 1312-1320.
Pushpa, K., Kumar, G. A. and Subramaniam, K. (2017). Translational control of germ cell decisions. In *Signaling-Mediated Control of Cell Division, Results and Problems in Cell Differentiation*, Vol. 59 (ed. S. Arur), pp. 175-200. Basel: Springer.
Rao, H. B. D. P., Qiao, H., Bhatt, S. K., Bailey, L. R. J., Tran, H. D., Bourne, S. L., Qiu, W., Deshpande, A., Sharma, A. N., Beebout, C. J. et al. (2017). A SUMO-ubiquitin relay recruits proteasomes to chromosome axes to regulate meiotic recombination. *Science* **355**, 403-407.
Sanford, C. and Perry, M. D. (2001). Asymmetrically distributed oligonucleotide repeats in the Caenorhabditis elegans genome sequence that map to regions important for meiotic chromosome segregation. *Nucleic Acids Res.* **29**, 2920-2926.
Sato, A., Isaac, B., Phillips, C. M., Rillo, R., Carlton, P. M., Wynne, D. J., Kasad, R. A. and Dernburg, A. F. (2009). Cytoskeletal forces span the nuclear envelope to coordinate meiotic chromosome pairing and synapsis. *Cell* **139**, 907-919.
Sonnichsen, B., Koski, L. B., Walsh, A., Marschall, P., Neumann, B., Brehm, M., Alleaume, A. M., Artelt, J., Bettencourt, P., Cassin, E. et al. (2005). Full-genome RNAi profiling of early embryogenesis in Caenorhabditis elegans. *Nature* **434**, 462-469.
Subramaniam, K. and Seydoux, G. (2003). Dedifferentiation of primary spermatocytes into germ cell tumors in C. elegans lacking the pumilio-like protein PUF-8. *Curr. Biol.* **13**, 134-139.
Takahashi, M., Iwasaki, H., Inoue, H. and Takahashi, K. (2002). Reverse genetic analysis of the Caenorhabditis elegans 26S proteasome subunits by RNA interference. *Biol. Chem.* **383**, 1263-1266.
Vaid, S., Ariz, M., Chaturbedi, A., Kumar, G. A. and Subramaniam, K. (2013). PUF-8 negatively regulates RAS/MAPK signalling to promote differentiation of C. elegans germ cells. *Development* **140**, 1645-1654.
Vilchez, D., Boyer, L., Morantte, I., Lutz, M., Merkwirth, C., Joyce, D., Spencer, B., Page, L., Masliah, E., Berggren, W. T. et al. (2012). Increased proteasome activity in human embryonic stem cells is regulated by PSMD11. *Nature* **489**, 304-308.
Woglar, A., Daryabeigi, A., Adamo, A., Habacher, C., Machacek, T., La Volpe, A. and Jantsch, V. (2013). Matefin/SUN-1 phosphorylation is part of a surveillance mechanism to coordinate chromosome synapsis and recombination with meiotic progression and chromosome movement. *PLoS Genet.* **9**, e1003335.
Yokoo, R., Zawadzki, K. A., Nabeshima, K., Drake, M., Arur, S. and Villeneuve, A. M. (2012). COSA-1 reveals robust homeostasis and separable licensing and reinforcement steps governing meiotic crossovers. *Cell* **149**, 75-87.
Zetka, M. C., Kawasaki, I., Strome, S. and Muller, F. (1999). Synapsis and chiasma formation in Caenorhabditis elegans require HIM-3, a meiotic chromosome core component that functions in chromosome segregation. *Genes Dev.* **13**, 2258-2270.

Supplemental material

PUF-8 facilitates homologous chromosome pairing by promoting proteasome activity during meiotic entry in *C. elegans*

Ganga Anil Kumar and Kuppuswamy Subramaniam

SUPPLEMENTARY METHODS

Genetic mapping of *kp23*

The *kp23* mutation was mapped to chromosome V through standard 2-factor crosses using the reference strains EG1000 (*dpy-5(e61) I; rol-6(e187) II; lon-1(e1820) III*) and EG1020 (*bli-6(sc16) IV; dpy-11(e224) V; lon-2(e678) X*). Briefly, the mutant strain IT859 was mated with the reference strains and the recombination frequency between the *kp23* allele and the marker mutations of the reference strains were calculated by determining the fraction number of F2 clones that yielded progeny having both *kp23* and the marker phenotypes. The mating scheme is given as a flowchart in Fig. S1. The recombination frequencies were: 63% for *dpy-5* (n=19); 100% for *rol-6* (n=19); 47% for *lon-1* (n=19); 47% for *bli-6* (n=21); 9% for *dpy-11* (n=21) and 81% for *lon-2* (n=21).

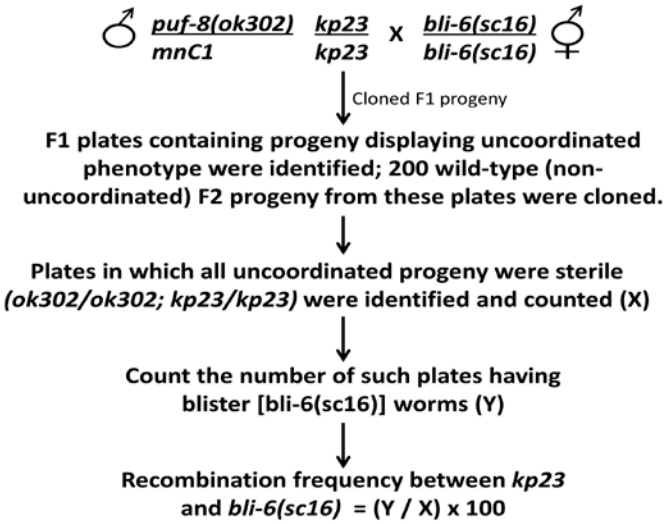

Fig. S1. Flow chart describing the 2-factor genetic crosses. The mating and recombination frequency calculation schemes with the *bli-6(sc16)* marker strain is shown here as an example. F2 worms were placed one hermaphrodite per plate (cloning) so that all F3 progeny present on a plate were from a single mother; thus, the genotype of the F2 worm could be inferred from the phenotypes of its progeny.

We performed whole genome sequencing and SNP analysis to further narrow down the position of *kp23* locus within chromosome V (Doitsidou et al., 2010). For this, we crossed IT859 worms with the polymorphic Hawaiian strain CB4586 and, by following the same strategy outlined in Fig. S1, selected the progeny of 27 cloned F2 worms that were homozygous for both *puf-8(ok302)* and *kp23*. These F2 progeny were pooled, and their genomic DNA was isolated and subjected to whole-genome sequencing. Genome sequencing and analysis were performed by GTAC, Washington University. As the DNA was isolated from worms homozygous for *kp23*, which is from N2 genetic background, CB4586-specific SNPs near the *kp23* locus is expected to be underrepresented in F2 *kp23* homozygotes. Indeed, CB4586-specific SNPs were particularly underrepresented between nucleotides 8,000,000 to 14,000,000 on chromosome V. Within this interval, there were nonsynonymous mutations affecting the coding sequences of *uig-1, pas-1, and coh-3*. RNAi-mediated depletion of UIG-1 and COH-3 in *puf-8(ok302)* worms did not show synthetic sterile phenotype; whereas depletion of PAS-1 by RNAi during larval stages caused *puf-8(ok302)*-dependent sterility, suggesting *kp23* might be an allele of *pas-1*. To further confirm the mapping results, we created the same G-to-A (substituting conserved glycine-20 with glutamic acid) change observed in *kp23* by CRISPR/Cas9 method; the resulting allele, named *kp72*, showed synthetic-sterile phenotype with *puf-8(ok302)* and the phenotype was indistinguishable from *puf-8(ok302); kp23* (Fig. S4).

Mapping *kp78*

To map *kp78*, we sequenced the genomes of *puf-8(ok302) unc-4(e120)/mnC1 II; pas-1(kp72) V; kp78* and *puf-8(ok302) unc-4(e120)/mnC1 II; pas-1(kp72) V* worms. Comparison of both genome sequences revealed changes in 29 genes. Of these, only *rpn-1* was predicted to encode a

proteasome component; therefore, we created the same mutation isolated by the genetic screen in the wild-type genetic background using the CRSIPR/Cas9 method (Fig. S11). The CRISPR allele, *kp85*, suppressed the *puf-8(ok302); pas-1(kp72)* phenotype, confirming that *kp78* is an allele of *rpn-1*.

Construction of strains:

Strains IT1205 and IT1011**:** IT859 [*puf-8(ok302) unc-4/mnC1; pas-1(kp23*)] males were mated with OP227 L4 hermaphrodites. From the progeny of this cross, F1 males were selected and mated with uncoordinated hermaphrodites (unc) (*puf-8 unc-4/puf-8 unc-4*) of JH1500. Progeny from this mating were cloned and allowed to lay progeny. From plates having 'unc' (75% fertile and 25% sterile), paralyzed dumpy (*mnC1/mnC1*), GFP-positive progeny, 64 worms were cloned. The plates in which all 'unc' progeny were fertile and GFP-positive and all 'unc' progeny were sterile and GFP-positive were selected as IT1205 and IT1011, respectively. Strains IT1013 and IT1119, IT1069 and IT1070, IT1017 and IT1016, IT1114 and IT1115 were generated as above by mating IT859 males with AV221, AV630, WH223 and CA1215 hermaphrodites, respectively.

IT1188*:* IT859 males were mated with IT1187 L4 hermaphrodites and the resulting progeny were cloned at the L4-stage. Based on parental genotypes, half of these L4s were expected to yield some 'unc' progeny while the other half, some paralyzed dumpy progeny. From the plates having 'unc' progeny, 64 worms were cloned. A plate in which all 'unc' progeny were sterile and some progeny were GFP-positive was selected, and 20 worms from that plate were cloned.

Of these 20, the ones that did not yield any 'unc' progeny, but produced progeny that were all GFP-positive, was selected as IT1188.

IT1210: IT859 males were mated with IT1153 L4 hermaphrodites. Male progeny of this cross were mated with IT1188 L4 hermaphrodites. From the resulting progeny, 16 L4 larvae were cloned. After 48 hours, the cloned worms were lysed and subjected to single-worm PCR using the primers KS5295 and KS5296 to identify worms carrying *rpn-1(kp78)* allele. Sixty four progeny of a worm positive for *rpn-1(kp78)* were cloned. Of these 64, the ones that yielded progeny that were all positive for both GFP and the *kp78* allele were selected.

IT966: IT859 males were mated with IT396 hermaphrodites. F2 progeny of this cross were cloned and selected for a plate in which all 'unc' progeny were sterile and all progeny were GFP-positive.

All strains used in this study are listed in Table S1.

Figure S2

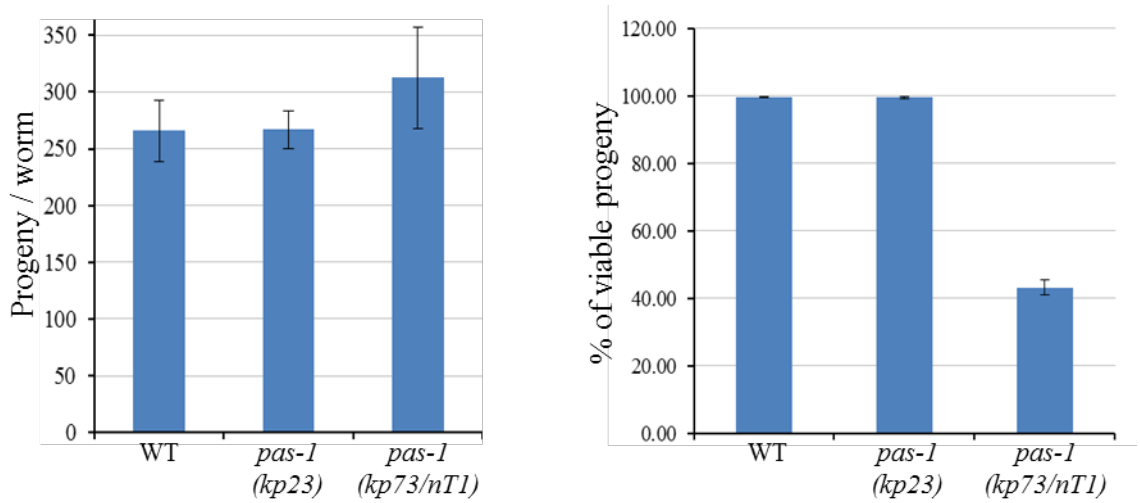

Fig. S2. Effect of *pas-1* alleles on brood-size and embryonic viability. The values are total number of embryos (left) and percentage of embryos that hatched (right) per worm of the indicated genotypes. In each case, the value represents the average from five worms. Note that the embryos homozygous for *nT1* are inviable; as a consequence, following Mendelian inheritance, 25% progeny of *pas-1(kp23)/nT1* are expected to be dead embryos due to *nT1*. Since about 60% progeny failed to hatch, all *kp73/73* homozygous and about 20% of *kp73/nT1* embryos were presumed to be dead due to the *kp73* mutation.

Figure S3

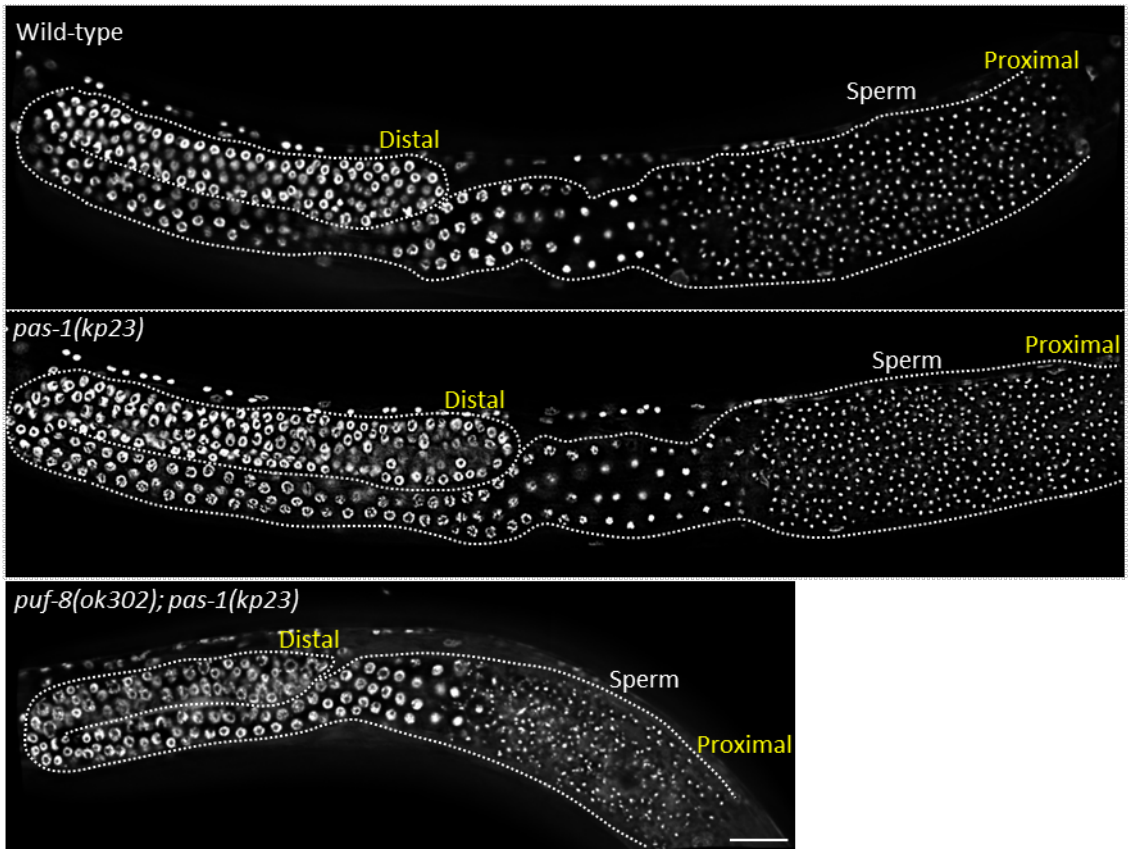

Fig. S3. The *kp23* mutation does not affect spermatogenesis in males. Adult males of the indicated genotypes were stained with DAPI. Germlines are outlined by dotted lines. Scale bar = 20µm.

Figure S4

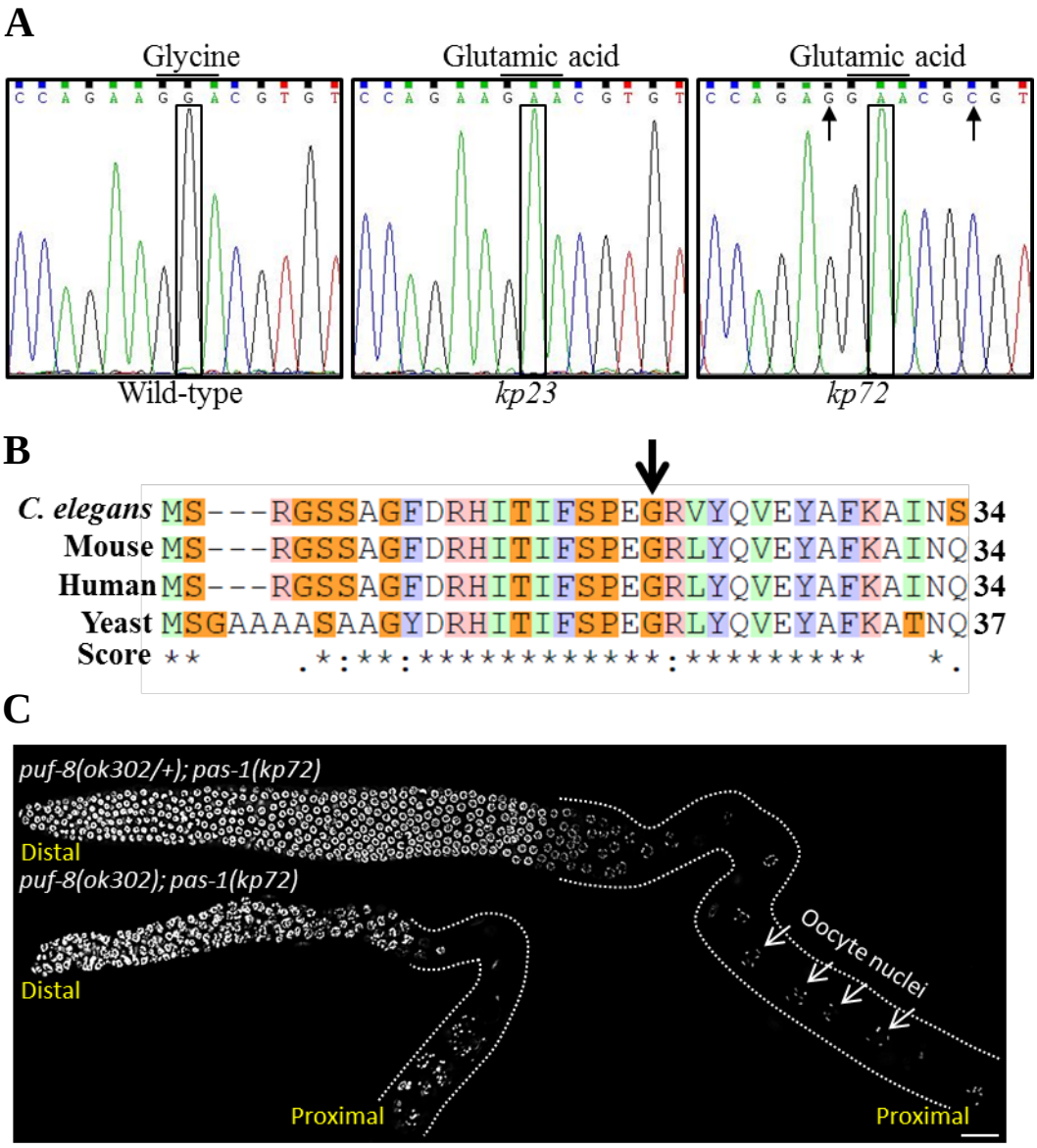

Fig. S4. *kp23* is an allele of *pas-1*. (A) Comparison of electropherograms of wild-type, *kp23*, *kp72* reveals a G-to-A change in the *pas-1* coding region of the mutant alleles. This single-base alteration replaces the conserved glycine residue at position 20 with glutamic acid. The arrows point to synonymous substitutions made to prevent re-cutting by Cas9. **(B)** Alignment of the N-terminal part of PAS-1 amino acid sequences. Arrow points to glycine-20. Asterisks, double-dots and single-dots mark perfectly conserved, highly conserved and semi-conserved residues, respectively. **(C)** Dissected gonads of the indicated genotypes stained with DAPI. Like the *puf-8(ok302); pas-1(kp23)* gonads, *puf-8(ok302); pas-1(kp72)* gonads do not have oocytes. Scale bar = 20µm.

Figure S5

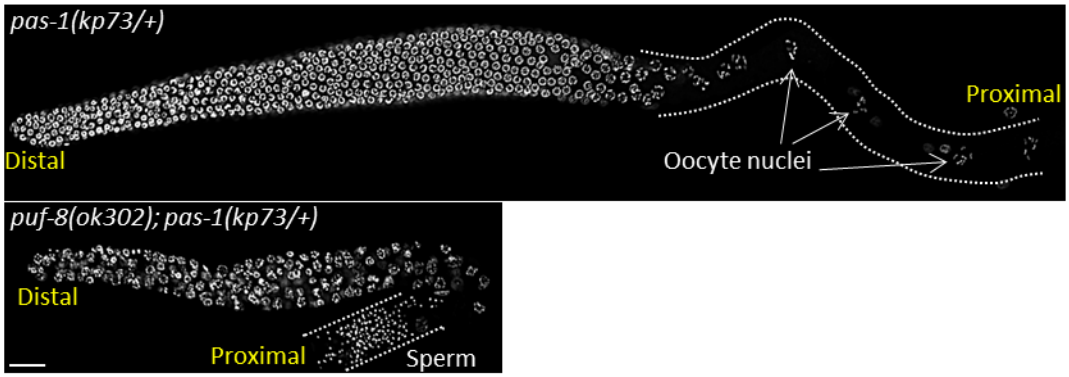

Fig. S5. The null allele, *kp73*, of *pas-1* exhibits haploinsufficient synthetic-sterility with *puf-8(ok302)*. Dissected gonads of the indicated genotypes stained with DAPI. Like the *puf-8(ok302); pas-1(kp23)* gonads (Fig. 1), *puf-8(ok302); pas-1(kp73/+)* gonads do not have oocytes. Scale bar = 20µm.

Figure S6

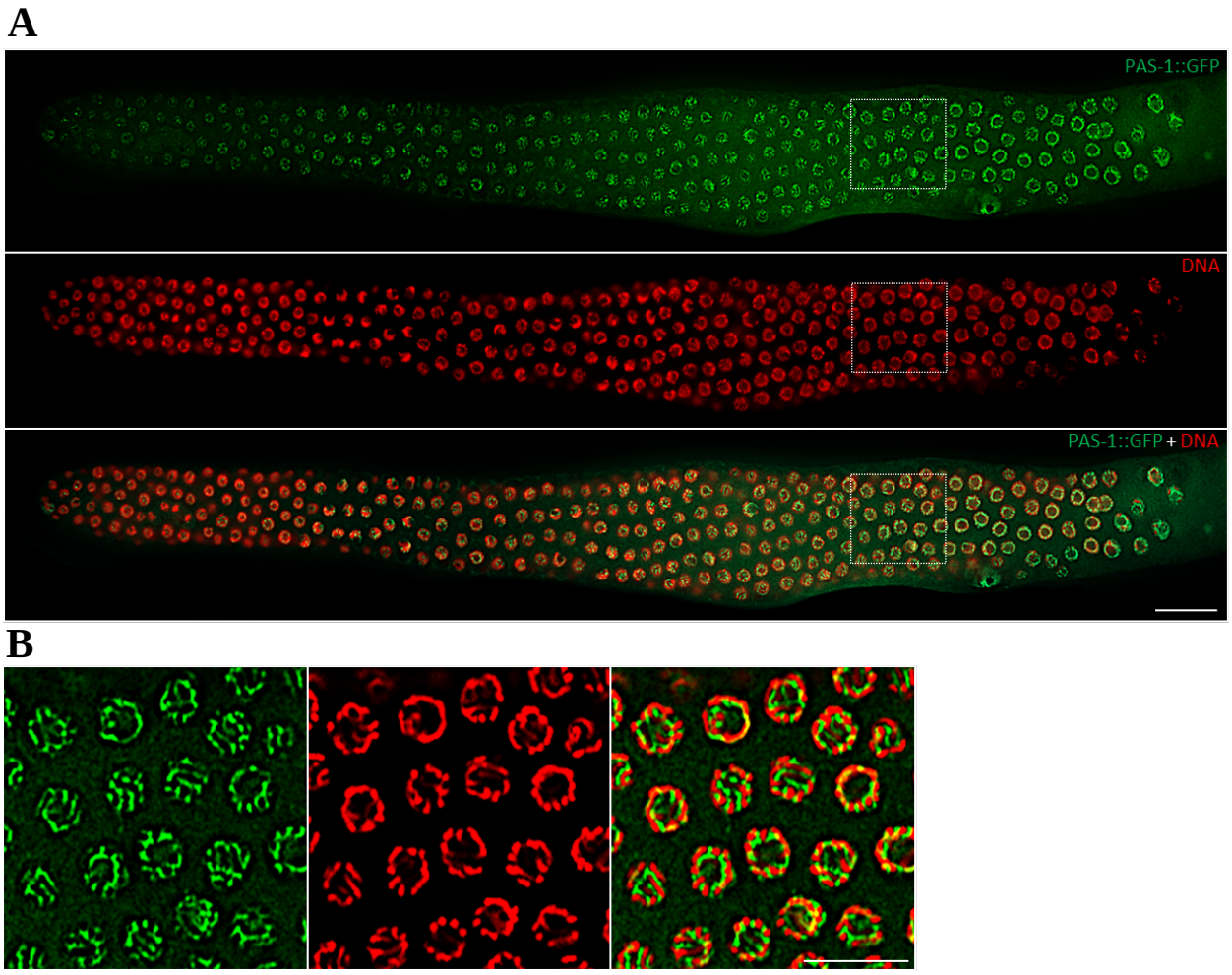

Fig. S6. Distribution pattern of PAS-1 in the germline. The presence of PAS-1 has been visualized by in-frame fusion of the GFP reporter at the C-terminus of PAS-1; coding sequences of GFP has been inserted at the endogenous *pas-1* locus using CRISPR/Cas9 method [strain IT1204]. **(A)** Distal arm of a dissected gonad stained with DAPI (red) is shown. Scale bar = 20µm. **(B)** Some pachytene nuclei [boxed area in **(A)**] are shown at higher magnification; PAS-1::GFP (green) localizes adjacent to chromatin (red). Scale bar = 10µm.

Figure S7

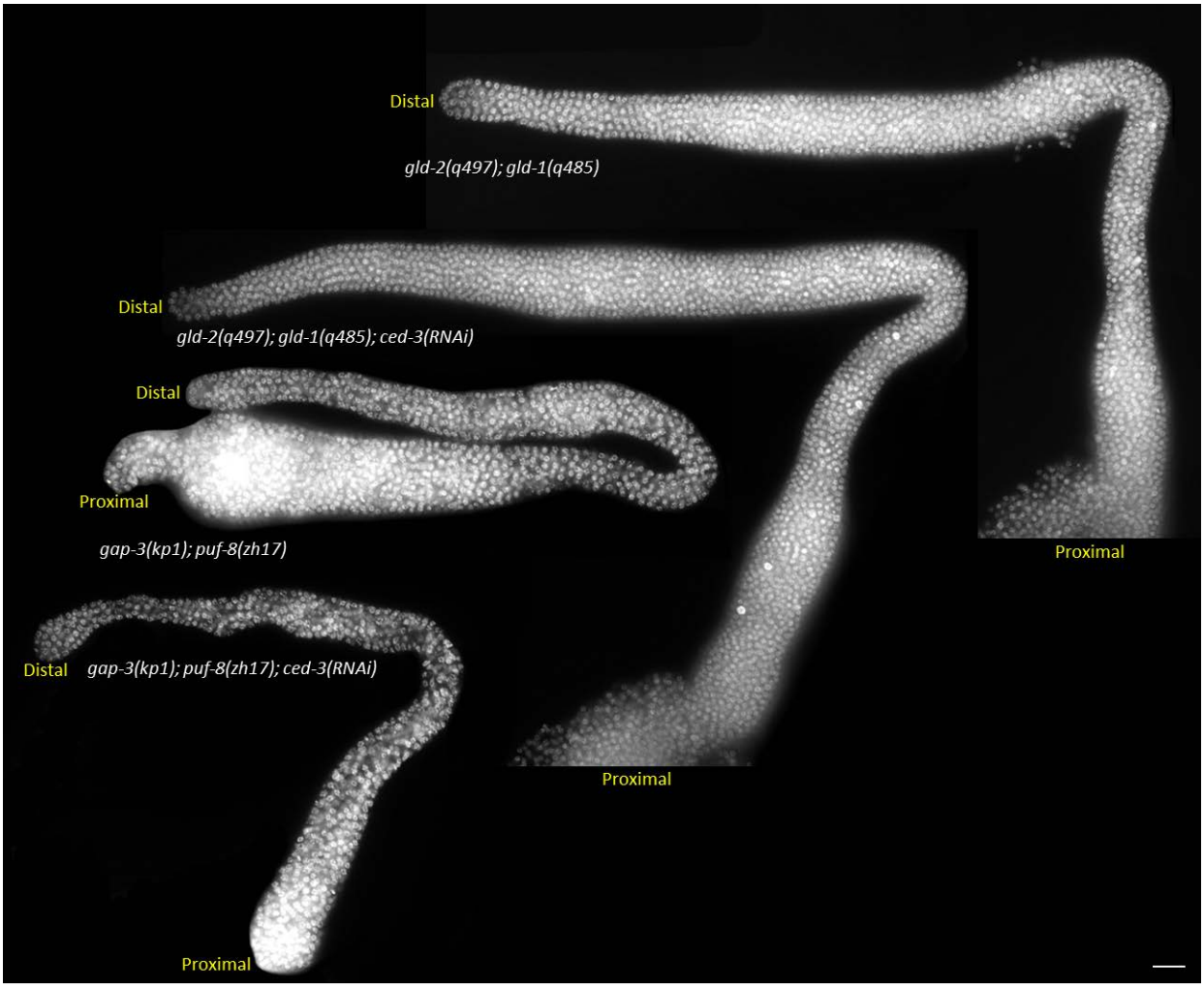

Fig. S7. Effect of blocking apoptosis on mutants defective for meiotic entry. Dissected gonads of the indicated genotypes stained with DAPI. In contrast to *puf-8(ok302); pas-1(kp23)* gonads (Fig. 2), *gld-2(q497) gld-1(q485)* and *gap-3(kp1); puf-8(zh17)* double mutants do not produce oocytes with univalent chromosomes upon inhibition of apoptosis by *ced-3(RNAi)*; instead, like the non-RNAi controls, they form germ cell tumor. For each genotype, 80 gonads were examined and all exhibited the same phenotype as shown here. Scale bar = 20µm.

Figure S8

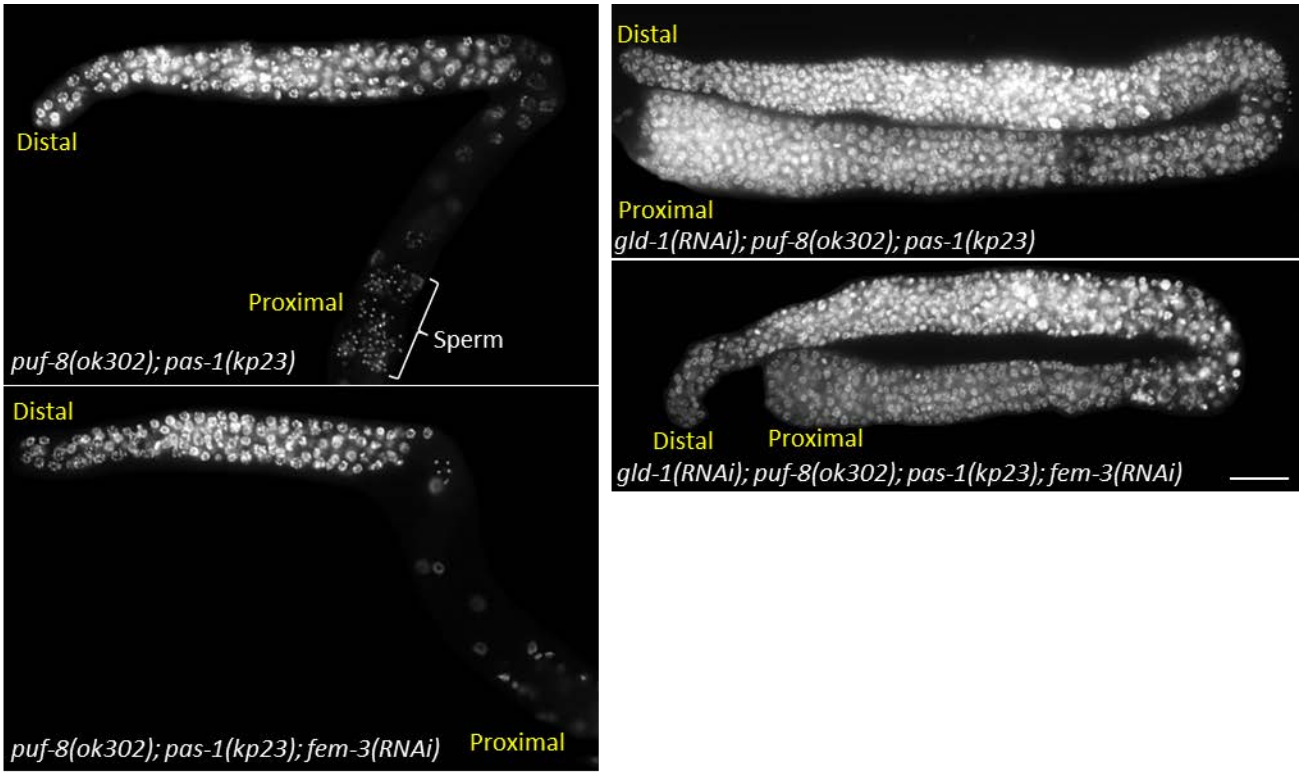

Fig. S8. Meiotic entry-dependent tumor development is not affected by *puf-8(ok302); pas-1(kp23)*. Dissected gonads of the indicated genotypes stained with DAPI. Female germ cells missing GLD-1 and male germ cells missing both GLD-1 and PUF-8 enter meiosis normally, but fail to progress through meiosis; instead, they dedifferentiate into germ cell tumors. Neither of these tumor formation is affected by *puf-8(ok302); pas-1(kp23)*, indicating that the *puf-8(ok302); pas-1(kp23)* germ cells enter meiosis normally. For each genotype, 80 gonads were examined and all exhibited the same phenotype as shown here. Scale bar = 20µm.

Figure S9

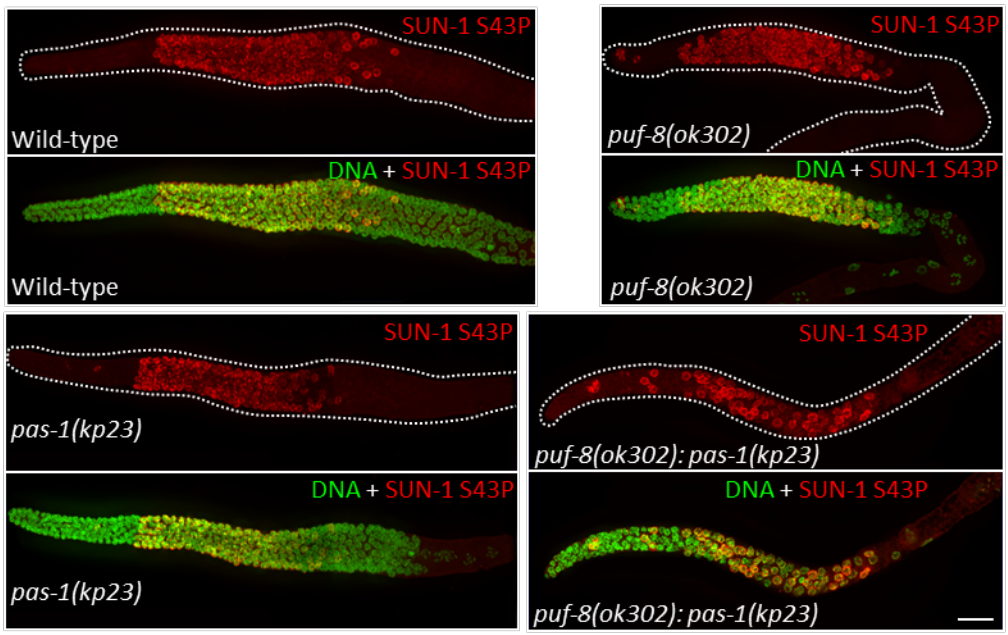

Fig. S9. SUN-1 phosphorylation is not affected by *puf-8(ok302); pas-1(kp23)*. Dissected gonads of the indicated genotypes stained with antibodies specific for SUN-1 phosphorylated at serine-43 (SUN-1 S43P) and DAPI. In the wild-type, as expected, germ nuclei stain positively for SUN-1 S43P upon meiotic entry. Similar immunostaining pattern is observed in the other three genotypes as well, which supports that the *puf-8(ok302); pas-1(kp23)* germ cells enter meiosis normally. Scale bar = 20µm.

Figure S10

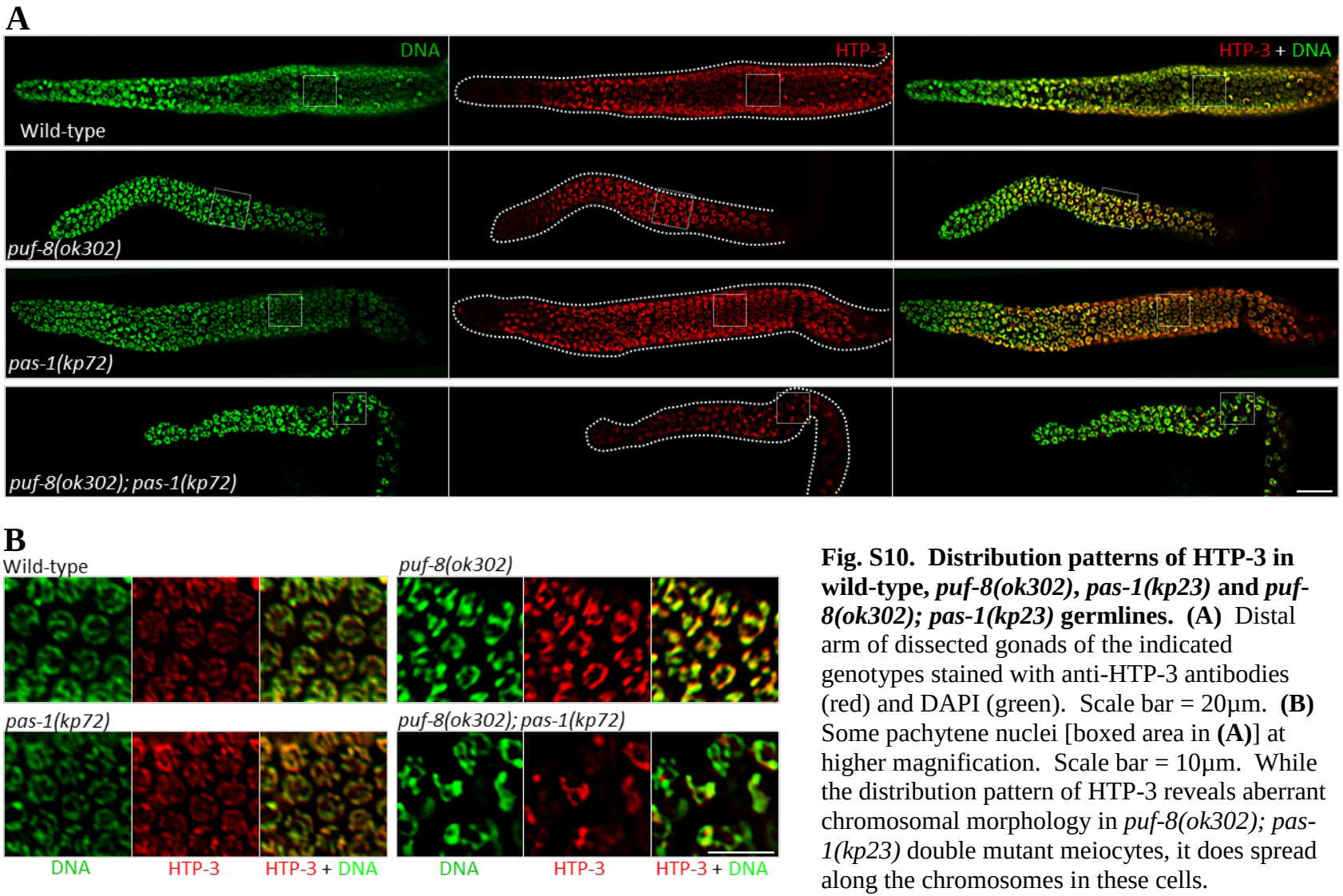

Fig. S10. Distribution patterns of HTP-3 in wild-type, *puf-8(ok302)*, *pas-1(kp23)* and *puf-8(ok302); pas-1(kp23)* germlines. (A) Distal arm of dissected gonads of the indicated genotypes stained with anti-HTP-3 antibodies (red) and DAPI (green). Scale bar = 20µm. **(B)** Some pachytene nuclei [boxed area in **(A)**] at higher magnification. Scale bar = 10µm. While the distribution pattern of HTP-3 reveals aberrant chromosomal morphology in *puf-8(ok302); pas-1(kp23)* double mutant meiocytes, it does spread along the chromosomes in these cells.

Figure S11

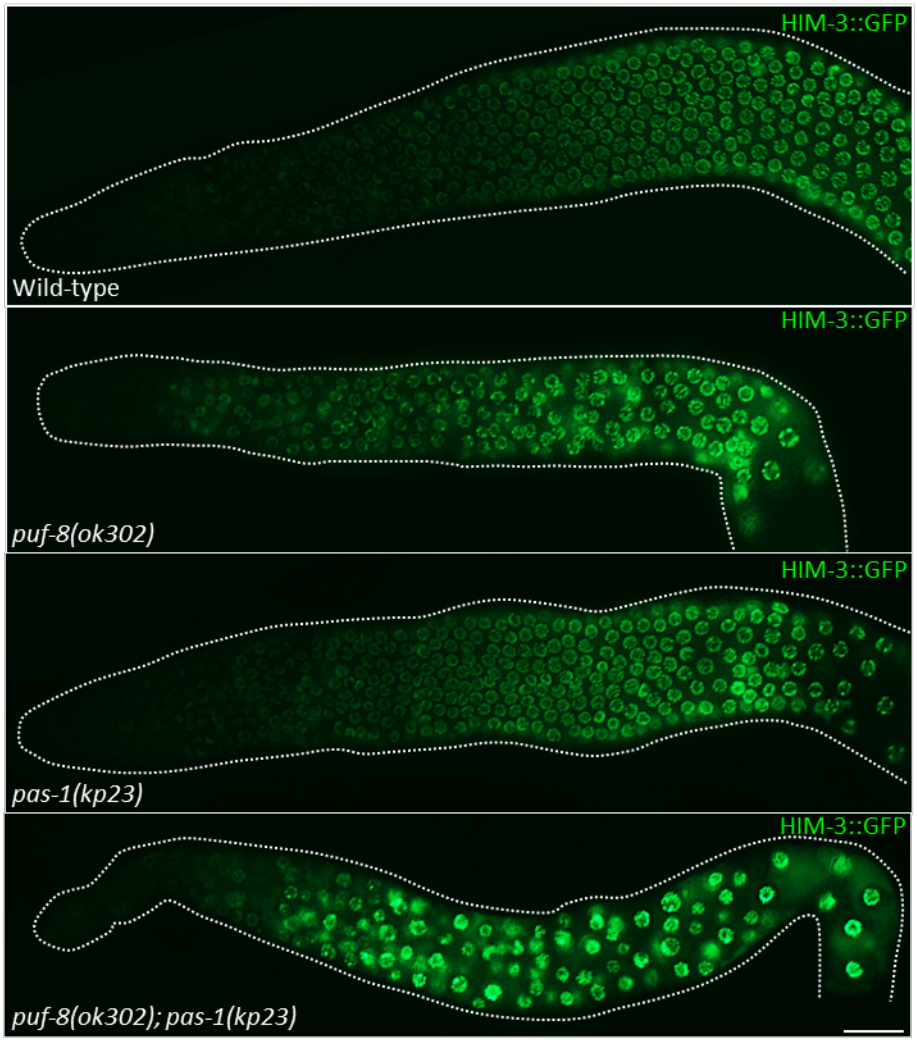

Fig. S11. Distribution patterns of HIM-3 in wild-type, *puf-8(ok302)*, *pas-1(kp23)* and *puf-8(ok302); pas-1(kp23)* germlines. Distal arm of dissected gonads of the indicated genotypes are shown [strains JH2120, IT396 and IT966]. The presence of HIM-3 has been visualized using a transgene that expresses HIM-3::GFP fusion protein (Merritt et al., 2008). Note that the onset of HIM-3::GFP expression is unaffected in the *puf-8(ok302); pas-1(kp23)* germline, although the fluorescence signal is somewhat brighter than the wild-type and reveals the aberrant chromatin morphology. Scale bar = 20µm.

Figure S12

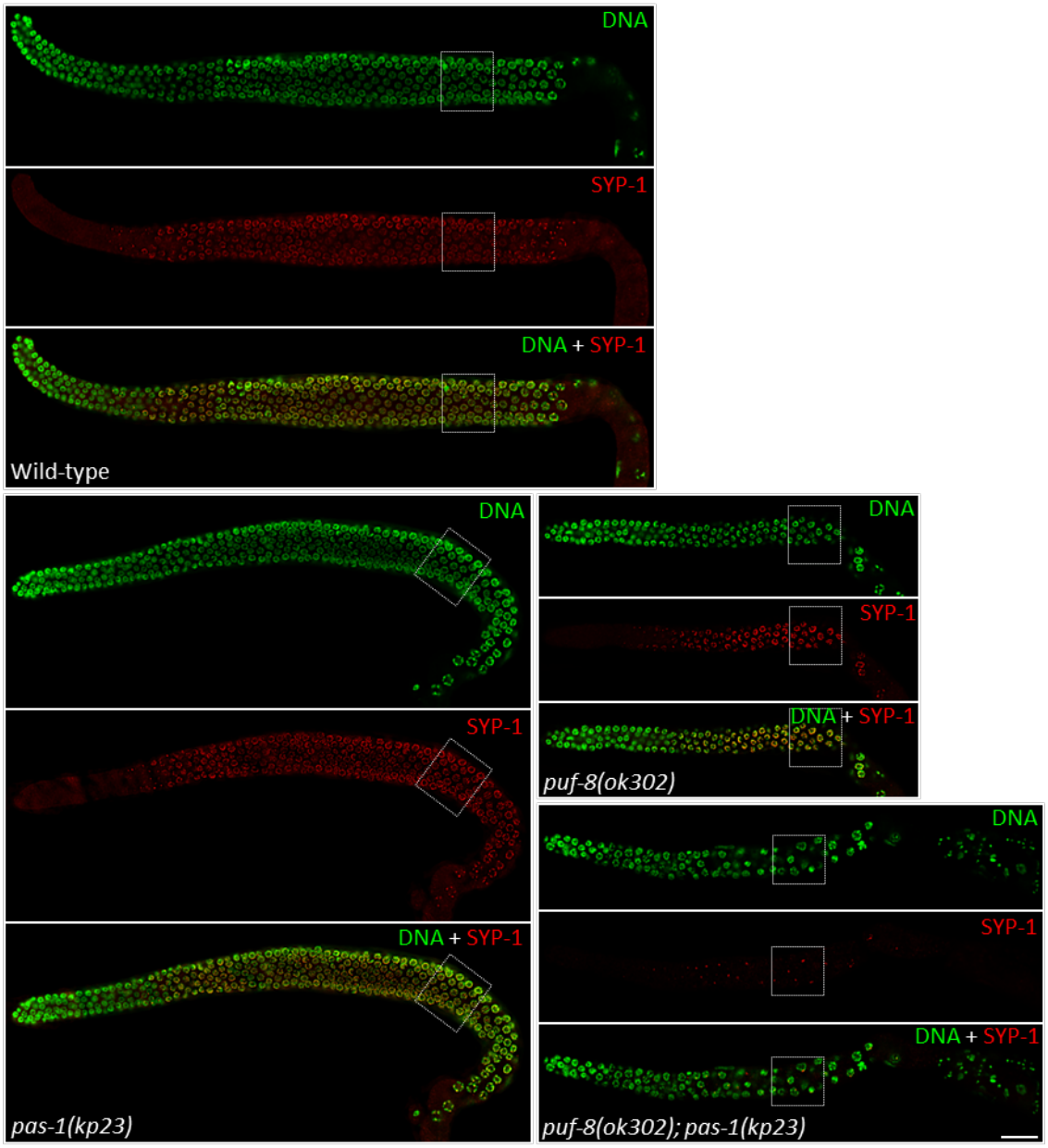

Fig. S12. Distribution patterns of SYP-1 in wild-type, *pas-1(kp23)*, *puf-8(ok302)* and *puf-8(ok302); pas-1(kp23)* germlines. Dissected gonads of the indicated genotypes stained with anti-SYP-1 antibodies (red) and DAPI (green) are shown. While SYP-1 spreads along meiotic chromatin in wild-type, *puf-8(ok302)* and *pas-1(kp23)* genotypes, it fails to spread and, instead, aggregates into specific foci in the *puf-8(ok302); pas-1(kp23)* double mutant. Boxed areas are shown at a higher magnification in Fig. 3. Scale bar = 20µm.

Figure S13

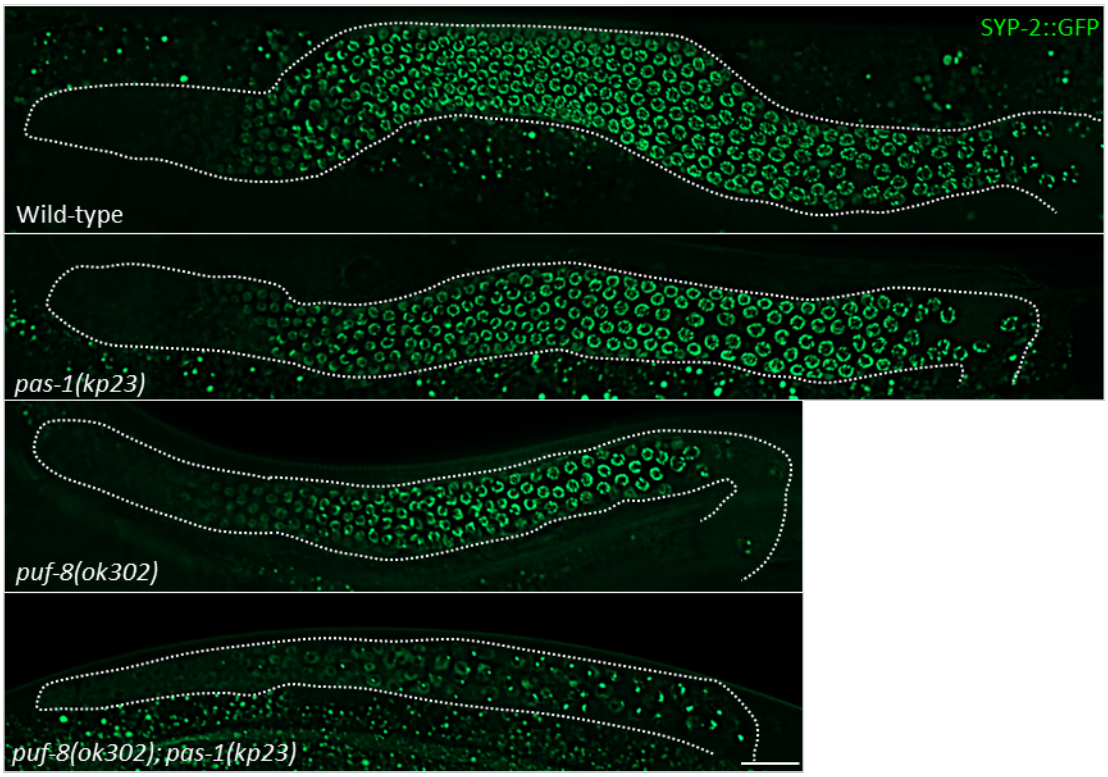

Fig. S13. Distribution patterns of SYP-2 in wild-type, *pas-1(kp23)*, *puf-8(ok302)* and *puf-8(ok302); pas-1(kp23)* germlines. Dissected gonads of the indicated genotypes expressing a transgene encoding SYP-2::GFP fusion protein are shown [strains OP227, IT1205 and IT1011]. Similar to SYP-1 aggregation (Fig. S9), SYP-2::GFP as well forms specific foci in the *puf-8(ok302); pas-1(kp23)* double mutant. Scale bar = 20µm.

Figure S14

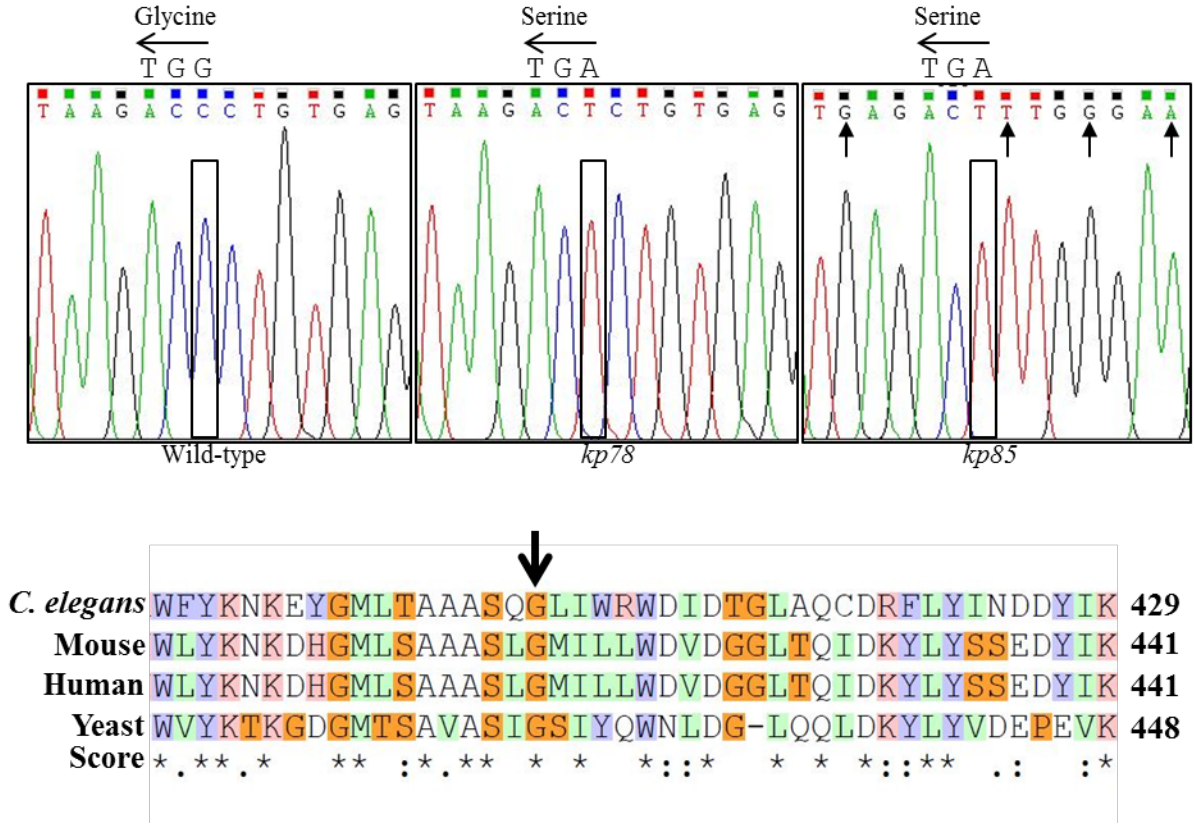

Fig. S14. *kp78* is an allele of *rpn-1*. (A) Comparison of electropherograms of wild-type, *kp78*, *kp85* reveals a G-to-A change in the *rpn-1* coding regions of the mutant alleles. This single-base alteration replaces the conserved glycine residue at position 403 with serine. Note that the electropherograms show the sequences of the non-coding strands. Arrows point to synonymous substitutions made to prevent re-cutting by Cas9. **(B)** Alignment of RPN-1 amino acid sequences around the region bearing the *kp78* mutation. Arrow points to glycine-403. Asterisks, double-dots and single-dots mark perfectly conserved, highly conserved and semi-conserved residues, respectively.

Table S1. List of *C. elegans* strains used in this study

Strain name	Genotype	Reference
JH1500	*puf-8(ok302) unc-4(e120)/mnC1 II*	(Subramaniam and Seydoux, 2003)
IT859	*puf-8(ok302) unc-4(e120)/mnC1 II; pas-1(kp23) V*	This study
IT1028	*puf-8(ok302) unc-4(e120)/mnC1 II; pas-1(kp72) V*	This study
IT1116	*puf-8(ok302) unc-4(e120)/mnC1 II; pas-1(kp73) V/nT1* [*qIs51*] *(IV;V)*	This study
OP230	*unc-119(ed3) III; wgIs230*[*syp-1::TY1::EGFP::3xFLAG(92C12) + unc-119(+)*]	(Gerstein et al., 2010; Sarov et al., 2006)
OP227	*unc-119(ed3) III; wgIs227*[*syp-2::TY1::EGFP::3xFLAG(92C12) + unc-119(+)*]	(Gerstein et al., 2010; Sarov et al., 2006)
IT1205	*puf-8(ok302) unc-4(e120)/mnC1 II; wgIs227*	This study
IT1011	*puf-8(ok302) unc-4(e120)/mnC1 II; pas-1(kp23) V; wgIs227*	This study
IT1153	*puf-8(ok302) unc-4(e120)/mnC1 II; rpn-1(kp78) IV; pas-1(kp72) V*	This study
IT1161	*puf-8(ok302) unc-4(e120)/mnC1 II; rpn-1(kp85) IV; pas-1(kp72) V*	This study
AV221	*unc-119(ed3) meT8 (III); meIs4 meT8 (IV); meIs1*	(Bilgir et al., 2013)
IT1013	*puf-8(ok302) unc-4(e120)/mnC1 II; meIs4 meT8 (IV); meIs1*	This study
IT1119	*puf-8(ok302) unc-4(e120)/mnC1 II; meIs4 meT8 (IV); pas-1(kp23) V; meIs1*	This study
AV630	*meIs8* [*pie-1p::GFP::cosa-1 + unc-119(+)*] *II*	(Yokoo et al., 2012)
IT1069	*puf-8(ok302) unc-4(e120)/mnC1 meIs8 II*	This study
IT1070	*puf-8(ok302) unc-4(e120)/mnC1 meIs8 II; pas-1(kp23) V*	This study
IT828	*unc-119(ed3) III; kpIs99* [*pie-1p::GFP::H2B::drp-1 3' UTR; unc-119(+)*]	This study
IT1187	*unc-119(ed3) III; kpIs100* [*pie-1p::Ub(G76V)::GFP::H2B::drp-1 3' UTR; unc-119(+)*]	This study
IT1188	*pas-1(kp23) V; kpIs100*	This study
IT1210	*rpn-1(kp78) IV; pas-1(kp23) V; kpIs100*	This study
IT1196	*htp-3(vc75) I; puf-8(ok302) unc-4(e120)/mnC1 II; pas-1(kp72) V*	This study
IT1204	*kpIs101* [*pas-1::GFP*] *V*	This study
CA1215	*dhc-1(ie28* [*dhc-1::degron::GFP*] *) I; ieSi38* [*sun-1p::TIR1::mRuby::sun-1 3'UTR + Cbr-unc-119(+)*] *IV*	(Zhang et al., 2015)
IT1114	*dhc-1(ie28*[*dhc-1::degron::GFP*]*) I; puf-8(ok302) unc-4(e120) /mnC1 II; ieSi38 IV*	This study
IT1115	*dhc-1(ie28*[*dhc-1::degron::GFP*]*) I; puf-8(ok302) unc-4(e120)/mnC1 II;ieSi38 IV; pas-1(kp23) V*	This study

WH223	*ojIs9* [*zyg-12(all)::GFP + unc-119(+)*]	(Malone et al., 2003)
IT1017	*puf-8(ok302) unc-4(e120)/mnC1 II; ojIs9*	This study
IT1016	*puf-8(ok302) unc-4(e120)/mnC1 II; pas-1(kp23) V; ojIs9*	This study
JH2120	*axIs1534* [*pie-1p::GFP::him-3 3'UTR + unc-119(+)*]	(Merritt et al., 2008)
IT396	*puf-8(ok302) unc-4(e120)/mnC1 II; axIs1534*	Unpublished
IT966	*puf-8(ok302) unc-4(e120)/mnC1 II; pas-1(kp23) V; axIs1534*	This study
JK2879	*gld-2(q497) gld-1(q485)/hT2 [bli-4(e937) let-?(q782) qIs48] (I;III)*	(Kadyk and Kimble, 1998)
IT540	*gap-3(kp1) I; puf-8(zh17) unc-4(e120)/mnC1 [dpy-10(e128) unc-52(e444)] II*	(Vaid et al., 2013)

Table S2. List of primers used in this study

Name	Sequence	Description
KS2431	CTTTCGGACAACATCTCGTG	Forward for *pas-3(RNAi)*
KS2432	TCTCAGCAGTCTCAGCTTCC	Reverse for *pas-3(RNAi)*
KS4565	CAACAGTTACGTCGAACCGC	Forward for *uig-1(RNAi)*
KS4566	AAGATGGAGTTGCACTGCTG	Reverse for *uig-1(RNAi)*
KS4567	ATATGCCATGCGAGCTTCTC	Forward for *pas-1(RNAi)*
KS4568	CGGTTGGCGATTTGATTGAG	Reverse for *pas-1(RNAi)*
KS4569	CGTTGAAGACGATTTGGCTG	Forward for *coh-3(RNAi)*
KS4570	TCTTCTGCTCCTTCGTTCTC	Reverse for *coh-3(RNAi)*
KS4631	CGTAGGAAATGAACAAAAGAGC	Reverse to detect *pas-1(kp72)* and *pas-1(kp73)*
KS4739	CAAGACATCTCGCAATAGG	Reverse for cloning sgRNA template into pDD162; for generating *kp72* mutation
KS4740	CCTGATAAACACGTCCTTCGTTTTAGAGCTAGAAATAGCAAGT	Forward primer used along with KS4739
KS4761	CAGCGCCGGATTCGATCGTCATATTACCATCTTCTCTCCAGAGGAACGCGTCTACCAGGTTATAAAATAATAGTTGAATGTTTATAAC	Repair template for *pas-1(kp72)*
KS4763	GAACTTCAATACGGCAAGATGAGAATGACTGGAAACCGTACCGCATGCGGTGCCTATGGTAGCGGAGCTTCACATGGCTTCAGACC	Repair template for *dpy-10(cn64)*
KS4764	TTTAAGGTGCGGTCACTCAA	Forward to detect *pas-1(kp72)* and *pas-1(kp73)*
KS4973	CAAAAAAAACTAGCAATAAAGGAATAAAAAACTGTACACCTTAAAGGCGC	Forward to amplify U6 promoter from pRB1017
KS4974	AAATTTCACAAAAAGCACCGACTCGGTGCC	Reverse to amplify U6 promoter from pRB1017
KS4998	GATTCGATCGTCATATTACCATCTTCTCTCCAAGCTAGCAGAAGGACGTGTTTATCAGGTTATAAAATAATAGTTGAATG	Repair template for *pas-1(kp73)*
KS5248	TCTTGTTACTGCAGCCGCCTCACA	Forward for sgRNA1 to make *rpn-1(kp78)*

KS5249	AAACTGTGAGGCGGCTGCAGTAAC	Reverse for sgRNA1 to make *rpn-1(kp78)*
KS5250	TCTTGCGCCTCACAGGGTCTTATC	Forward for sgRNA2 to make *rpn-1(kp78)*
KS5251	AAACGATAAGACCCTGTGAGGCGC	Reverse for sgRNA2 to make *rpn-1(kp78)*
KS5252	TCTTGCTCCAGATAAGACCCTGTG	Forward for sgRNA3 to make *rpn-1(kp78)*
KS5253	AAACCACAGGGTCTTATCTGGAGC	Reverse for sgRNA3 to make *rpn-1(kp78)*
KS5261	AAGAACAAGGAATATGGAATGCTTACTGCAGCCGC TTCCCAAAGTCTCATTTGGAGATGGGATATCGATAC CGGCCTGGCACAATGC	Repair template for *rpn-1(kp78)*
KS5295	GCTTACTGCAGCCGCTTCCCAAA	To detect *rpn-1(kp78)*
KS5296	GGATCAGGAAGTGAACGGAG	To detect *rpn-1(kp78)*
KS5428	TCTTGGATACCGTCGACCTCGAGG	Forward for sgRNA1 to insert ub(G76V) into IT1828
KS5429	AAACCCTCGAGGTCGACGGTATCC	Reverse for sgRNA1 to insert ub(G76V) into IT1828
KS5430	TCTTGACCGTCGACCTCGAGGGGG	Forward for sgRNA2 to insert ub(G76V) into IT1828
KS5431	AAACCCCCCTCGAGGTCGACGGTC	Reverse for sgRNA2 to insert ub(G76V) into IT1828
KS5432	ATGGGATCCCCCGGGCTGCAGGAATTCGATATCAA GCTTATCGATACCGTCGACCTCGAGATGCAGATCTT CGTGAAGAC	Forward for ub(G76V), template for CRSIPR/Cas9
KS5433	GACAACTCCAGTGAAAAGTTCTTCTCCTTTACTCAT TTTTTCTACCGGTACCGCCCCCACCACACCTCTGAG ACGGAGTA	Reverse for ub(G76V), template for CRSIPR-Cas9
KS5565	TCTTGATGAATATTTAATCTCGGT	Forward for sgRNA1 at the C-terminus of *pas-1*
KS5566	AAACACCGAGATTAAATATTCATC	Reverse for sgRNA1 at the C-terminus of *pas-1*
KS5567	TCTTGGTCGATGAATATTTAATCT	Forward for sgRNA2 at the C-terminus of *pas-1*
KS5568	AAACAGATTAAATATTCATCGACC	Reverse for sgRNA2 at the C-terminus of *pas-1*
KS5576	TCTGCAGGATCCAACTCTACCAATCTGACGGC	Forward for 5′ homology arm (repair template) of *pas-1*
KS5577	TCTGCAGGATCCATCTCGGTTGGCGATTTGATTGAG ATGATGTTCGACCTGATCGCTAGTTAGCTTAGTGAA TTTGGAGTTATCCTTGGTGAC	Reverse for 5′ homology arm (repair template) of *pas-1*
KS5584	TTCGAAGCTTTTGGCGTCAT	Forward primer to detect *htp-3(vc75)*
KS5585	TGAATTTCGAGGCATATGCG	Reverse primer to detect *htp-3(vc75)*

Supplementary references

Bilgir, C., Dombecki, C. R., Chen, P. F., Villeneuve, A. M. and Nabeshima, K. (2013). Assembly of the Synaptonemal Complex Is a Highly Temperature-Sensitive Process That Is Supported by PGL-1 During Caenorhabditis elegans Meiosis. *G3 (Bethesda)* **3**, 585-595.

Doitsidou, M., Poole, R. J., Sarin, S., Bigelow, H. and Hobert, O. (2010). C. elegans mutant identification with a one-step whole-genome-sequencing and SNP mapping strategy. *PLoS One* **5**, e15435.

Gerstein, M. B. Lu, Z. J. Van Nostrand, E. L. Cheng, C. Arshinoff, B. I. Liu, T. Yip, K. Y. Robilotto, R. Rechtsteiner, A. Ikegami, K. et al. (2010). Integrative analysis of the Caenorhabditis elegans genome by the modENCODE project. *Science* **330**, 1775-87.

Kadyk, L. C. and Kimble, J. (1998). Genetic regulation of entry into meiosis in Caenorhabditis elegans. *Development* **125**, 1803-13.

Malone, C. J., Misner, L., Le Bot, N., Tsai, M. C., Campbell, J. M., Ahringer, J. and White, J. G. (2003). The C. elegans hook protein, ZYG-12, mediates the essential attachment between the centrosome and nucleus. *Cell* **115**, 825-36.

Merritt, C., Rasoloson, D., Ko, D. and Seydoux, G. (2008). 3' UTRs are the primary regulators of gene expression in the C. elegans germline. *Curr. Biol.* **18**, 1476-82.

Sarov, M., Schneider, S., Pozniakovski, A., Roguev, A., Ernst, S., Zhang, Y., Hyman, A. A. and Stewart, A. F. (2006). A recombineering pipeline for functional genomics applied to Caenorhabditis elegans. *Nat Methods* **3**, 839-44.

Subramaniam, K. and Seydoux, G. (2003). Dedifferentiation of primary spermatocytes into germ cell tumors in C. elegans lacking the pumilio-like protein PUF-8. *Curr. Biol.* **13**, 134-9.

Vaid, S., Ariz, M., Chaturbedi, A., Kumar, G. A. and Subramaniam, K. (2013). PUF-8 negatively regulates RAS/MAPK signalling to promote differentiation of C. elegans germ cells. *Development* **140**, 1645-54.

Yokoo, R., Zawadzki, K. A., Nabeshima, K., Drake, M., Arur, S. and Villeneuve, A. M. (2012). COSA-1 reveals robust homeostasis and separable licensing and reinforcement steps governing meiotic crossovers. *Cell* **149**, 75-87.

Zhang, L., Ward, J. D., Cheng, Z. and Dernburg, A. F. (2015). The auxin-inducible degradation (AID) system enables versatile conditional protein depletion in C. elegans. *Development* **142**, 4374-84.